Check for updates

The Meteoritical Society

Meteoritics & Planetary Science 1–21 (2024)
doi: 10.1111/maps.14225

High-resolution cathodoluminescence of calcites from the Cold Bokkeveld chondrite: New insights on carbonatation processes in CM parent bodies

Vincent GUIGOZ[1,*], Anthony SERET[2], Marc PORTAIL[1], Ludovic FERRIÈRE[3], Guy LIBOUREL[2,4], Harold C. CONNOLLY Jr[5,6,7], and Dante S. LAURETTA[6]

[1]CNRS, CRHEA, Université Côte d'Azur, Valbonne, France
[2]Observatoire de la Côte d'Azur, CNRS, Laboratoire Lagrange, Université Côte d'Azur, Nice, France
[3]Natural History Museum Abu Dhabi, Abu Dhabi, United Arab Emirates
[4]Hawai'i Institute of Geophysics and Planetology, School of Ocean, Earth Science and Technology, University of Hawai'i at Mānoa, Honolulu, Hawai'i, USA
[5]Department of Geology, Rowan University, Glassboro, New Jersey, USA
[6]Lunar and Planetary Laboratory, University of Arizona, Tucson, Arizona, USA
[7]Department of Earth and Planetary Science, American Museum of Natural History, New York, New York, USA

***Correspondence**
Vincent Guigoz, CNRS, CRHEA, Université Côte d'Azur, Rue Bernard Grégory, Valbonne 06560, France.
Email: vincent.guigoz@crhea.cnrs.fr

(Received 18 July 2023; revision accepted 28 May 2024)

Abstract–Carbonates, as secondary minerals found in CM chondrites, have been widely employed for reconstructing the composition of the fluids from which they precipitated. They also offer valuable insights into the hydrothermal evolution of their parent bodies. In this study, we demonstrate that high-resolution cathodoluminescence (HR-CL) analyses of calcites derived from the brecciated Cold Bokkeveld CM2 chondrite can effectively reveal subtle compositional features and intricate zoning patterns. We have identified two distinct types of cathodoluminescence (CL) centers: a blue emission band (approximately 375–425 nm), associated with intrinsic structural defects, and a lower energy orange extrinsic emission (around 620 ± 10 nm), indicating the presence of Mn cations. These compositional variations enable discrimination between the calcite grain types previously designated as T1 and T2 in studies of CM chondrites. T1 calcites exhibit variable CL and peripheral Mn enrichments, consistently surrounded by a rim composed of Fe-S-rich serpentine–tochilinite assemblage. Conversely, T2 calcites display homogeneous CL and more abundant lattice defects. These polycrystalline aggregates of calcite grains, devoid of serpentine, contain Fe-Ni sulfide inclusions and directly interface with the matrix. We propose that changes in the Mn content of calcite (indicated by the intensity of orange CL emission) are influenced by variations in redox potential (Eh) and pH of the fluid phase. This proposed hydrothermal evolution establishes a parallel between terrestrial serpentinization followed by carbonation processes and the aqueous alteration of CM chondrites, warranting further exploration and investigation of this intriguing similarity.

INTRODUCTION

Recent observations of near-Earth asteroid [101955] Bennu by the OSIRIS-REx mission revealed spectral evidence of widespread carbonates, as well as high-reflectance, centimeter-thick, meter-long linear features within boulders interpreted as hydrothermally deposited carbonate veins (Kaplan et al., 2020; Lauretta et al., 2022). The first mineralogical results obtained on Bennu samples confirm the occurrence of carbonates

© 2024 The Author(s). *Meteoritics & Planetary Science* published by Wiley Periodicals LLC on behalf of The Meteoritical Society.
This is an open access article under the terms of the Creative Commons Attribution License, which permits use, distribution and reproduction in any medium, provided the original work is properly cited.

(Lauretta, 2023), which will help us to better constrain the geologic history of carbonaceous asteroids especially their past hydrothermal activities.

Cathodoluminescence (CL), the emission of photons (ultraviolet to near-infrared) following injection of high-voltage electrons in a mineral, has long been recognized as a powerful technique to explore many fundamental properties of $CaCO_3$, including insights into crystal growth, zonation, deformation, trace elements, and defect structure, as well as its modes and its physico-chemical conditions of formation (Barker & Cox, 2011; Götze, 2012; Lee et al., 2005; Pagel et al., 2000; Toffolo et al., 2019). Most of the photons fall in the visible portion of the electromagnetic spectrum (wavelengths of 400–700 nm) with some falling in the ultraviolet (UV) and infrared (IR) portions of the electromagnetic spectrum. The luminescence of carbonate minerals is primarily dependent on the abundance of Mn^{2+} activators. However, the presence of Fe^{2+} plays a crucial role as a "quencher," causing the creation of non-radiative de-excitation pathways for excited carriers. This phenomenon leads to the quenching of mineral luminescence. More specifically, the different emission's center of luminescence in $CaCO_3$ is caused by (i) substitutions of Mn^{2+} for Ca^{2+}; (ii) substitutions of rare earth elements (REE) for Ca^{2+}; (iii) dislocations of the $[CO_3]^{2-}$ anions; (iv) oxygen vacancies and broken Ca-O bonds (Habermann et al., 1998; Pagel et al., 2000; Metzler et al., 1992; see discussion below). CL characterization thus provides insights, not available by other research techniques, into detailed crystal chemistry and growth modes of carbonates.

To evaluate whether the chemistry of the Bennu-returned samples is distinct from that of our corpus of meteorites, we have launched a high-resolution cathodoluminescence (HR-CL) survey of carbonates in several carbonaceous chondrites. Since prior to the samples returned to the Earth, the Mighei-type CM chondrites were amongst the closest spectral analogs to the surfaces of Bennu (Binzel et al., 2015; DellaGiustina et al., 2021; Hamilton et al., 2019; Lauretta et al., 2022) we report here results on carbonates, mainly calcites of the Cold Bokkeveld CM2 carbonaceous chondrite. Cold Bokkeveld is classified as CM2.1–2.7 and is an impact regolith breccia that shows significant inter- and intrasample mineralogical heterogeneity (Bischoff et al., 2017; Lentfort et al., 2020). Because its clasts experienced various degrees of aqueous alteration, it was chosen as an appropriate training meteorite for this study.

The CM chondrites are chemically among the most primitive extraterrestrial materials available for study (e.g., Brearley, 2006). The CM parent body(ies) is (are) thought to originate beyond the so-called snowline in the protoplanetary disk (~1–3 AU). As a result, they accreted ices that melted early in solar system history, producing fluids (Miyamoto, 1991) that led to varying degrees of aqueous alteration. This process transformed pristine anhydrous silicates, metal, sulfide, and other accessory phases into secondary minerals comprised of abundant (>60 vol%) phyllosilicates with minor amounts (<5 vol %) of oxides, sulfides, carbonates, and organic compounds (e.g., Howard et al., 2009, 2011). The most characteristic secondary phases in CM chondrites are tochilinite–cronstedtite intergrowths (TCIs), occurring as complex assemblages dispersed throughout the matrix (Fuchs et al., 1973; Howard et al., 2015; Lentfort et al., 2020; Nakamura & Nakamuta, 1996; Palmer & Lauretta, 2011; Rubin et al., 2007; Tomeoka & Buseck, 1985). The mineralogical and chemical characteristics of CM chondrites indicate that the aqueous alteration proceeded at low temperatures (<200/300°C) during the first ~6 million years of the solar system (Fujiya et al., 2012; Visser et al., 2020).

In CM chondrites, several carbonate species are present. The most abundant phase is calcite, with minor amounts of dolomite, aragonite, and breunnerite (Lee et al., 2012, 2014; Riciputi et al., 1994). It is generally accepted that calcite precipitated from the fluid phase, initially infilling void space, forming vugs, and acting as a cement. Later generations of calcite grew upon existing secondary phases or replaced primary anhydrous silicates. It is also assumed that early alteration produced Fe-bearing calcite while later alteration favored the precipitation of Mg-bearing calcite (Lee et al., 2014). Calcite mineralization in CM chondrites has been shown to be complex, with episodic growth periods interrupted by dissolution.

Two main populations of calcite are recognized (Lee et al., 2013; Lindgren et al., 2017; Riciputi et al., 1994; Tyra et al., 2012, 2016; Vacher et al., 2017, Vacher, Piralla, et al., 2019). The T1 calcites are characterized by small grain sizes and are always mantled by a rim composed of serpentine and tochilinite. The T2 calcites are larger, multigrain aggregates that are free of phyllosilicate–tochilinite rims. Instead, they are surrounded by fine-grained matrix and are often associated with sulfide grains. The first generation of calcites (T1) formed before the main growth windows for phyllosilicate and sulfides (e.g., Vacher, Piralla, et al., 2019). These early calcites may have coprecipitated with other complex carbonates (e.g., breunnerite) facilitated by the presence of increasingly Mg-rich solutions (Lee et al., 2012). Meanwhile, the later generation of calcites (T2) formed after phyllosilicates and sulfides (Lindgren et al., 2017; Suttle et al., 2021; Vacher, Piralla, et al., 2019). The second-generation T2 calcites also replaced primary ferromagnesian silicates as well as infilling fractures to form veins (Lee et al., 2013).

Based on the O-isotope composition of carbonates (Clog et al., 2024; Guo & Eiler, 2007), the reconstructed

19455100, 0, Downloaded from https://onlinelibrary.wiley.com/doi/10.1111/maps.14225 by Universite Cote D'azur, Wiley Online Library on [11/06/2024]. See the Terms and Conditions (https://onlinelibrary.wiley.com/terms-and-conditions) on Wiley Online Library for rules of use; OA articles are governed by the applicable Creative Commons License

alteration temperatures for calcites are in the range of 0–250°C with the T1 calcites formed at low temperatures (<100°C) while T2 calcites formed at higher temperatures (100–250°C, see Vacher, Piralla, et al., 2019). Accordingly, it is assumed that alteration in CM parent body(ies) operated along a prograde thermal path (increasing temperatures with time), concurrent with a decreasing W/R ratio, as water was progressively consumed in hydration reactions (Rosenberg et al., 2001).

Concerning the Cold Bokkeveld chondrite, the modal mineralogy of the bulk sample, determined by X-ray diffraction (Howard et al., 2009, 2011), comprises serpentine (77.4 vol%), olivine (11.5 vol%), pyroxene (4.9 vol%), sulfides (3.0 vol%), magnetite (2.0 vol%), calcite (1.0 vol%), and gypsum (0.8 vol%). Carbonates from Cold Bokkeveld have received a lot of attention (Farsang et al., 2021; Lee et al., 2013, 2014; Verdier-Paoletti et al., 2017; among others). However, the most recent study by Farsang et al. (2021) reveals the existence of carbonates displaying petrographic features that are distinct from those of T1 and T2 carbonates commonly observed in CM2 meteorites, including carbonates interstitial to octahedral magnetite crystals. At least six stages of potentially overlapping carbonate and phyllosilicate formation events are indicated. The diverse compositions and petrographic features of carbonates and associated phases are interpreted as indicative of precipitation from locally formed, physically restricted aqueous fluids that only penetrated through small regions (Farsang et al., 2021).

Does the presence of carbonates exhibiting diverse petrographic features suggest the occurrence of multiple generations of fluids on each clast parent body, potentially resulting from the heterogeneity of accreted ices and mineral assemblages within Cold Bokkeveld clasts? Or did they result from the compositional evolution of fluids on a single parent body? Are temperature variations deduced from isotopic analyses the main variable controlling carbonate formation? Focusing on calcite, the most abundant carbonate mineral in CM chondrites, here we show that HR-CL helps answer these questions and decipher the crystallization history of carbonates shedding a new light on hydrothermal activity in chondrite parent bodies.

MATERIAL AND ANALYTICAL

Sample Characterization

The Cold Bokkeveld meteorite is a carbonaceous chondrite that fell in many pieces near the Cold Bokkeveld Mountains, in Cape Province, South Africa, on October 13, 1838. The Cold Bokkeveld thin section NHMW-O1128 used here was provided by the Natural History Museum Vienna (Figure 1). At the first glance, the optical map of the section (≈4 cm^2) confirms that Cold Bokkeveld is a chondrite breccia hosting various lithologies with a range of size. Numerous cracks and one vein are also present. The various degrees of alteration recorded by each of these fragments led Lentfort et al. (2020) to propose an extended classification scheme based on that of Rubin et al. (2007, mainly based on the "FeO"/SiO_2 ratio of TCIs), including the fragments with the highest (e.g., 2.1, 2.2) and lowest degree of alteration (e.g., 2.8, 2.9). Cold Bokkeveld is hence classified as a CM 2.1–2.7. Lentfort et al. (2020) also suggested that the range of aqueous alteration in CM chondrites and small spatial scale of mixing of clasts with different alteration histories will be important for interpreting returned Bennu samples, which our study on Cold Bokkeveld confirms.

X-Ray Chemical maps

The general overview of Cold Bokkeveld thin section NHMW-O1128 with coupled backscattered electron (BSE) images and energy-dispersive X-ray (EDX) spectroscopy chemical maps was acquired at CEMEF Mines ParisTech-Nice (France) with a MEB FEI XL30 environmental scanning electron microscope (ESEM) LaB6. Measurements were operated at 20 kV and 200 nA beam current, equipped with a BRUKER Quantax 655 detector with XFlash 6|30 technology silicon drift 10 mm^2 at 129 eV (100 kcps). BRUKER Microanalyzer QUANTAX was associated with the software ESPRIT (semiquantitative analyses without standard by P/B-ZAF method).

High-Resolution Cathodoluminescence

The high-resolution CL (HR-CL) facility consists of a MonoCL4 GATAN system equipped with both a high-sensitivity array detector (UV enhanced Pixis100 camera) and a high-sensitivity photomultiplier mounted on a field emission gun scanning electron microscope (FEG-SEM; JEOL JSM7000F at CRHEA, Valbonne, France) and suitable both for hyperspectral analyses and panchromatic imaging. The electron beam current used in the study ranged typically from 1 to 4 nA. Panchromatic images were acquired at 3 keV, for a spatial resolution at the nanometer scale, with a scanning rate of 700 µs/pixel. Filtered panchromatic images were made using bandpass filter from Thorlabs centered on 400 ± 20 nm and 620 ± 10 nm. For spectral and hyperspectral analyses, the luminescence coming from the excited sample is directed toward a Czerny–Turner type 300 mm focal length monochromator equipped with 150 grooves/mm grating blazed at 500 nm; the entrance slit has been fixed to 300 µm, which gives a spectral

19455100, 0, Downloaded from https://onlinelibrary.wiley.com/doi/10.1111/maps.14225 by Universite Cote D'azur, Wiley Online Library on [11/06/2024]. See the Terms and Conditions (https://onlinelibrary.wiley.com/terms-and-conditions) on Wiley Online Library for rules of use; OA articles are governed by the applicable Creative Commons License

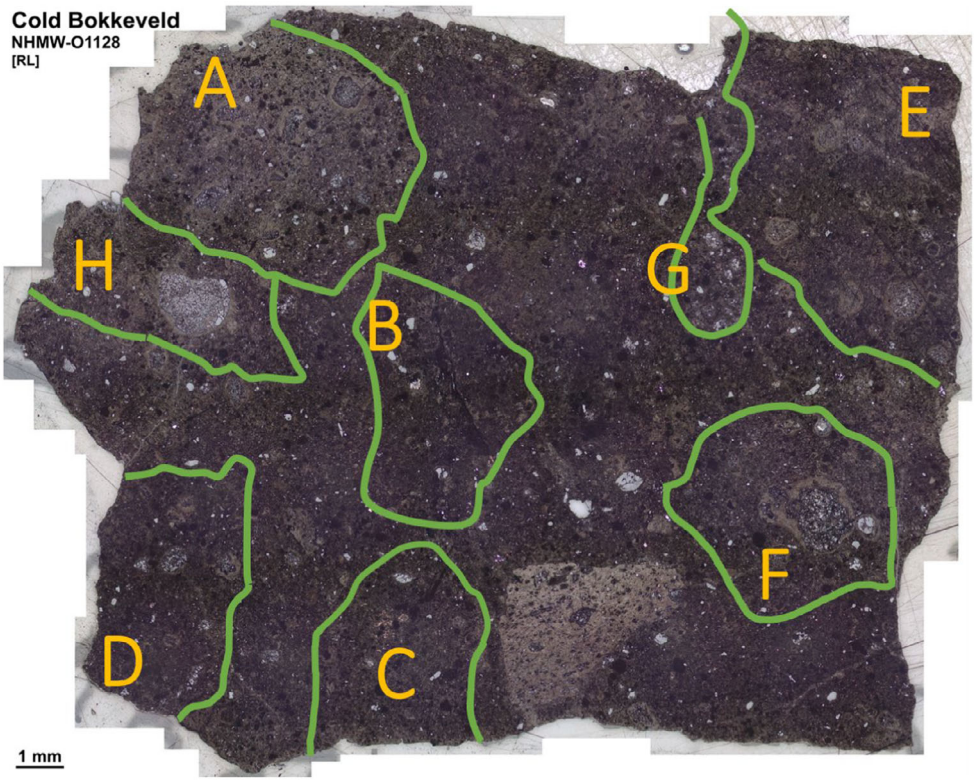

FIGURE 1. Optical microscopy reflected light image of the NHMW-O1128 Cold Bokkeveld CM2 thin section showing clasts, identified with letter A to H and their borders highlighted in green, and the brecciation process of this chondrite.

resolution better than 3 nm. Dispersed light is collected as a whole using the CCD detector having a sensitivity range from 250 to 1050 nm. Excited photons under a 5-keV beam were integrated for 20 s. All measurements and observations were done at room temperature.

Electron Microprobe Analysis (EMPA)

Elemental quantitative point and maps analyses were performed using a JEOL JXA 8230 electron microprobe equipped with five wavelength-dispersive spectrometers (WDS) at the Institut des Sciences de la Terre (ISTerre, Grenoble, France). Point analysis of major elements (Fe, Mn, Mg, Sr, Ca, C, and Cr) was acquired using an acceleration voltage of 15 kV, a beam current of 50 nA, a dwell time of 20 ms, and a spot size of 10 μm. The X-ray maps of major elements were acquired using an acceleration voltage of 15 kV, a beam current of 90 nA, and a dwell time of 0.2 ms. The JEOL software ZAF method was used for matrix corrections. Calcite reference material was used for major element standardization and for monitoring analytical accuracy and precision during measurements (see supplementary material).

RESULTS

Maps, Clasts, and Carbonates

The optical (Figure 1) and X-ray maps (Figures 2 and S2) presented here are a combination of Fe (green channel), Ca (red channel), and Al (blue channel) of the studied thin section. This map confirms the presence of various clasts characterized by different size, mineralogy, and chemistry emerging within the continuous matrix of the Cold Bokkeveld chondrite. We did not attempt classification of each clast based on their degree of alteration, but we confirmed that these clasts show very different degrees of alteration (Lentfort et al., 2020). This is suggested by variations of the Fe/Si ratio of the hydrated phases (see image processing of Fe and Si X-ray individual maps in the supplementary material) covarying with the alteration indicator of "FeO"/SiO_2 ratio of TCIs following the method proposed by Rubin et al. (2007). In this respect, the comparison between the clasts labeled G and E (see supplementary materials) provides an exemplary study of the effect of aqueous alteration on carbonate mineral chemistry.

19455100, 0, Downloaded from https://onlinelibrary.wiley.com/doi/10.1111/maps.14225 by Universite Cote D'azur, Wiley Online Library on [11/06/2024]. See the Terms and Conditions (https://onlinelibrary.wiley.com/terms-and-conditions) on Wiley Online Library for rules of use; OA articles are governed by the applicable Creative Commons License

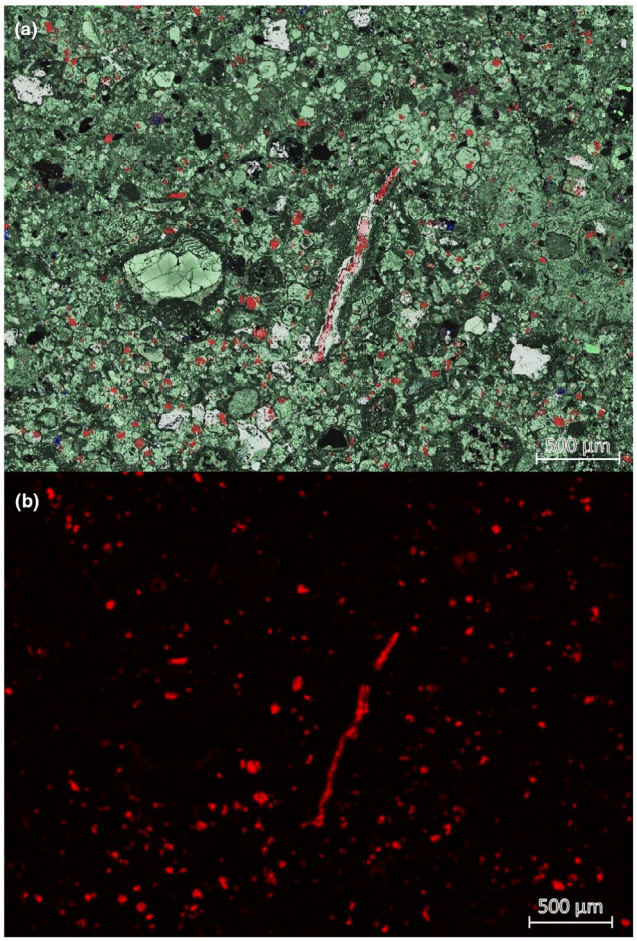

FIGURE 2. (a) Blended BSE and EDX map (Ca = red, Fe = green and Al = blue) and (b) corresponding elemental Ca EDX map of Cold Bokkeveld displaying a vein of calcite and isolated T1 calcite grains.

While several carbonates including aragonite, calcite, and dolomite have already been documented in the Cold Bokkeveld chondrite, we have focused our study on calcite as it is the most abundant of the carbonate phases (e.g., Farsang et al., 2021). Despite the lithological heterogeneity of the meteorite, calcite grains are ubiquitous (Figures 2–4 and S2, Table S1). While exhibiting significant variation in modal abundances across clasts, ranging from nearly absent carbonates (e.g., Clast G) to up to 3%–5% (e.g., Clast E), no clear relationship with the degree of alteration is evident (see Figure S3). Image processing using ImageJ of X-ray maps of the bulk thin section gives an estimate of 0.8 ± 0.1% for calcite modal proportions, consistent with those calculated by XRD on bulk powders of this meteorite, that is, ≈1% (Howard et al., 2011).

Calcite grains appear equant, although some form more complex ring structures (Figure 5 and supplementary material). Only one occurrence of calcite veins has been observed in the studied section (Figure 2, with its location indicated by a red dotted square on Figure S2). The great majority of the calcites are rimmed by a more-or-less continuous and thick (5–10 µm) serpentine/tochilinite assemblage, making them easily recognizable as T1-type calcites (Lee et al., 2014; Tyra et al., 2007, 2012). T1 calcites range in size from ten to a few tens of micrometers, with an average size between 50 and 60 µm (Figure 4). Calcite grains in the continuous matrix of the Cold Bokkeveld are smaller than those in clasts, on average (Figures 2 and 3). Rarer T2 calcite grains are observable in clasts and possibly in matrix (Figure 4o). They differ morphologically from T1 calcites by being comprised of polycrystalline porous aggregates sprinkled with Fe-Ni sulfide inclusions and lacking serpentine rims. The main petrographic characteristic of both T1 and T2 calcites of the Cold Bokkeveld chondrite we observed are similar to those already described in previous studies (De Leuw et al., 2010; Farsang et al., 2021; Lee et al., 2013; Lentfort et al., 2020; Sofe, 2013).

Carbonate Chemical Composition

We analyzed several T1 and T2 calcite grains in different clasts (Table S1; Figure S4). Systematic electron beam damages have been observed after analyses in calcites (Figure S1). T1 calcite grains contain only minor amounts of MgO and MnO. The highest measured MgO concentration is 1.3 wt%. The MnO contents vary from values below the detection limits to values as high as 0.8 wt%. MnO contents are positively related to the measured MgO concentration and are generally higher than MgO. All analyzed carbonate grains contain moderate amounts of FeO (between 0.6 and 2.5 wt%). No obvious correlation between FeO and MnO can be, however, seen in this set of calcite analyses. These data are very similar to those reported by De Leuw et al. (2010) and Tyra et al. (2012). T2 calcite grains have composition close to that of T1 populations (see also Tyra et al., 2012, for the composition of T2 calcites from EET 96016 and EET96006 CM2 chondrites). They differ by a lower Mn content and poor correlations with both Fe and Mg. MnO rarely exceeds 0.1 wt% and no peripheral enrichment in MnO have been measured in T2 calcite grains.

Panchromatic HR-CL Images of Carbonates

In panchromatic CL images, the gray scale represents the sum of photons emitted at all wavelengths, with brighter gray translating to a higher number of photons received by the photomultiplier. The high sensitivity of our CL system coupled with the high-spatial resolution of an

19455100, 0, Downloaded from https://onlinelibrary.wiley.com/doi/10.1111/maps.14225 by Universite Cote D'azur, Wiley Online Library on [11/06/2024]. See the Terms and Conditions (https://onlinelibrary.wiley.com/terms-and-conditions) on Wiley Online Library for rules of use; OA articles are governed by the applicable Creative Commons License

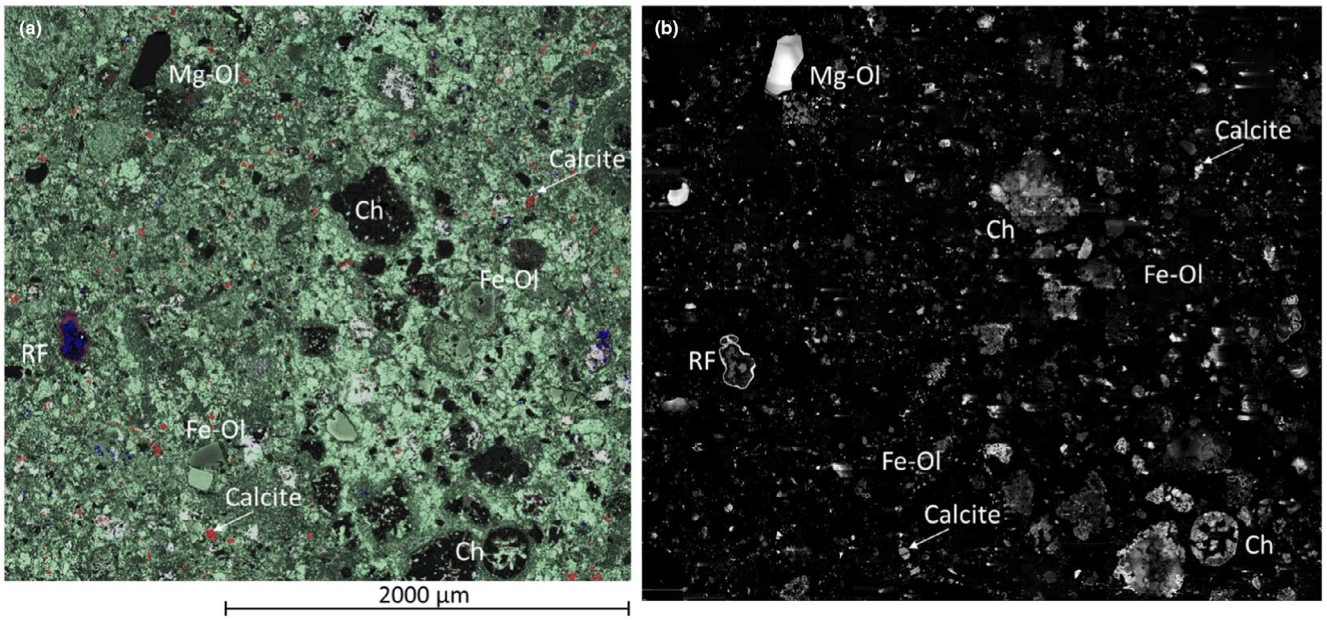

FIGURE 3. Comparison between (a) blended X-ray elemental map in Ca (red), Fe (green), and Al Kα (blue) and (b) panchromatic high-resolution cathodoluminescence (HR-CL) image in the central region of the section (Figure 2) near the G clast. This example shows how HR-CL panchromatic maps allow to identify materials sensitive to the cathodoluminescence (type I chondrules (Ch), isolated forsterites, refractory inclusions (RF), AOAs, magnesium-rich olivine (Mg-Ol), iron-rich olivine (Fe-Ol), etc.) from those, generally iron rich, that are not; here an efficient way of confirming the high modal abundance of iron-bearing oxides/hydroxides in the Cold Bokkeveld mineralogy.

FEG-SEM allows us to resolve very faint compositional features that would otherwise have remained invisible at the submicrometer scale using standard BSE imaging. Both millimeter- or micrometer-sized panchromatic HR-CL images can be acquired.

Large areas can be mapped, allowing identification of luminescent materials (Figure 3). In the example shown in Figure 3, Mg-rich forsterite from chondrules (Lauretta et al., 2022; Libourel & Portail, 2018; Libourel et al., 2022) and amoeboid olivine aggregates (AOA), low-Ca-pyroxene from chondrules, spinel and anorthite from refractory inclusions and carbonates from secondary phases in the matrix can be easily recognized by comparison with the X-ray chemical map. Most of the area does not emit photons, however. This is due to the high concentration of iron hosted in ferroan olivine from chondrules and mainly in the overabundant intergrowths of cronstedtite–tochilinite assemblages and other iron-bearing oxides/hydroxides constituting the clasts and the chondrite matrix; an indirect way of confirming the high modal abundance of iron-bearing phyllosilicates in the Cold Bokkeveld mineralogy (Howard et al., 2011) as a first approximation. At this scale, carbonates can be recognized only by coupling the Ca X-ray chemical map to the CL one. As revealed by this correlation, their modal abundances vary significantly from one clast to another (Figures 2, 3 and supplementary material).

At the micron scale, carbonates exhibit variable CL intensity evidencing complex internal zoning, almost impossible to detect with classical BSE-SEM images. In the studied section, more than 80 calcite grains have been documented in the matrix and across the different clasts (see Figure S6 in Supplementary Material). While this survey did not have any statistical purpose, the CL heterogeneity of these carbonates deserves to be highlighted (Figure 4).

In Cold Bokkeveld, T1 calcite grains are monocrystalline or polycrystalline. In the former case, calcite occurs as anhedral and subhedral crystals clearly showing their cleavage and/or twin networks. In the latter, calcites are made of coarse polycrystalline aggregates with unaltered grain boundaries. Grains are very often equant. In either case, CL panchromatic images reveal calcite grains with different intensities of zonation, and some with clear core to edge concentric zoning (Figure 4). In concentrically zoned calcites, the CL intensity generally decreases from core to edge (Figure 5 and supplementary material). In the same type of grains, the CL intensity may show oscillatory zones, alternating bands of high and low CL intensity without any marked trend toward grain core or edge (Figures 6 and S6), suggesting asymmetric growth. It should be noted that, in both cases, the HR-CL panchromatic images acquired in just a few minutes provide a better

19455100, 0, Downloaded from https://onlinelibrary.wiley.com/doi/10.1111/maps.14225 by Universite Cote D'azur, Wiley Online Library on [11/06/2024]. See the Terms and Conditions (https://onlinelibrary.wiley.com/terms-and-conditions) on Wiley Online Library for rules of use; OA articles are governed by the applicable Creative Commons License

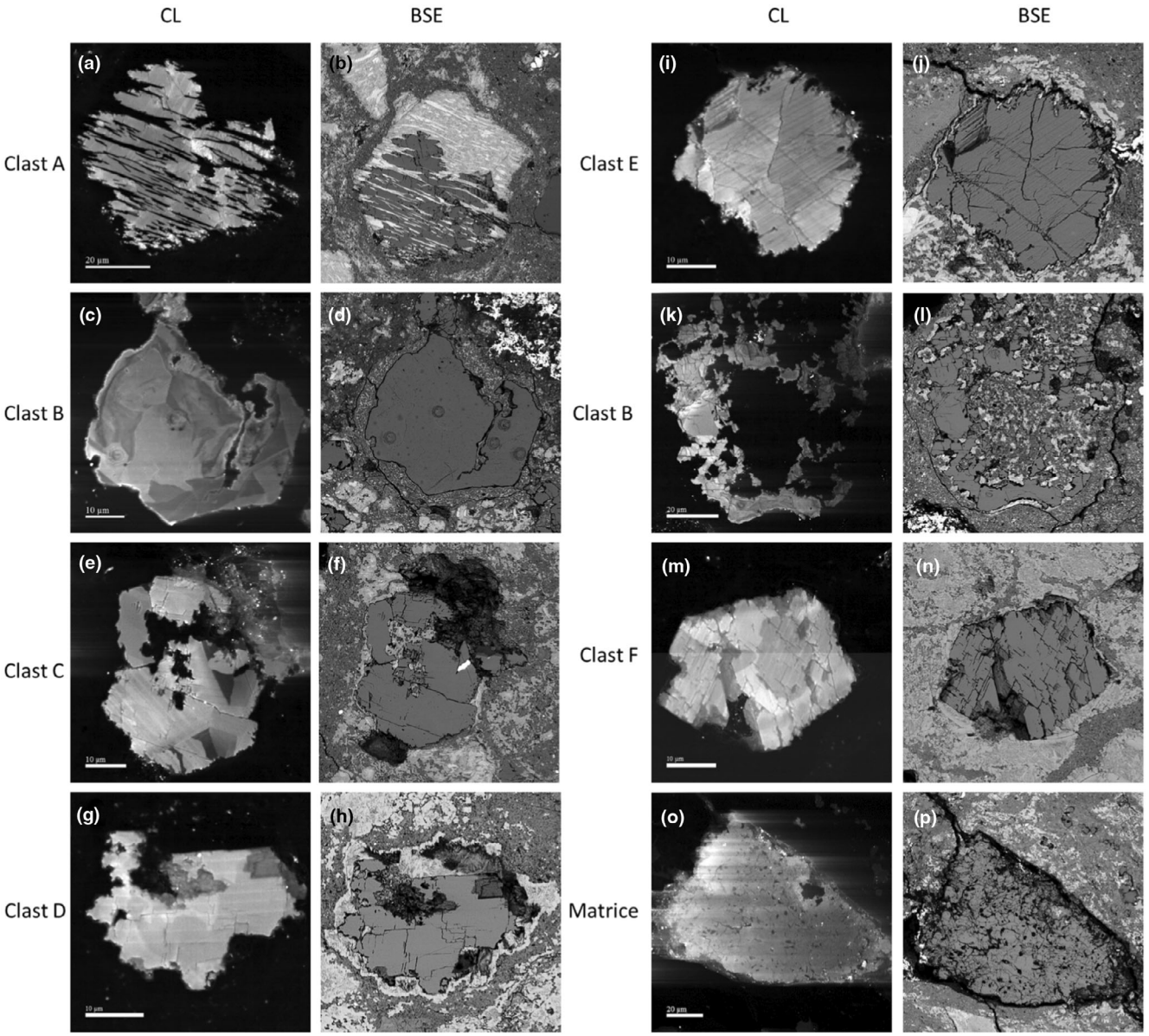

FIGURE 4. BSE map (b, d, f, h, j, l, n and p) and HR-CL panchromatic image (a, c, e, g, i, k, m and o) of representative T1 calcites sampled in the different clasts and of a T2 calcite (o) from the matrix of Cold Bokkeveld CM2 chondrite. Notice how HR-CL is able to resolve faint compositional features that would otherwise have remained invisible at the sub-micrometer scale using standard BSE imaging. See text for description.

resolution than that obtained by EMPA X-ray map after 14 h of analyses, without commensurate beam damage (Figure S1). Finally, other grains exhibit irregular CL intensity delineating different patches with blurred contours, suggesting complex growth processes (Figure 4c,e,m as examples). In contrast, T2 calcites are porous, multigrain aggregates associated with sulfides. Although rare, they are easily recognizable by their homogeneous but weak CL intensity (Figure 4o). However, special attention must be paid to the observed surfaces because even minor roughness can significantly affect the luminescence intensity and consequently modify the CL panchromatic images.

T1 calcites are often rimmed by finely intertwined serpentine/tochilinite with occasional evident tochilinite fibers. The thickness of this rim varies from very thin (<1 μm) to quite thick (20–30 μm). It is also common for calcite grains that are included in serpentine/tochilinite assemblages to occur as regular alternations of carbonate and hydrated phases (C101–C104 in Figure S6 Supplementary Material). In rarer cases, finely polycrystalline and microporous T2 calcite aggregates, lacking the serpentine/tochilinite rims, are

19455100, 0, Downloaded from https://onlinelibrary.wiley.com/doi/10.1111/maps.14225 by Universite Cote D'azur, Wiley Online Library on [11/06/2024]. See the Terms and Conditions (https://onlinelibrary.wiley.com/terms-and-conditions) on Wiley Online Library for rules of use; OA articles are governed by the applicable Creative Commons License

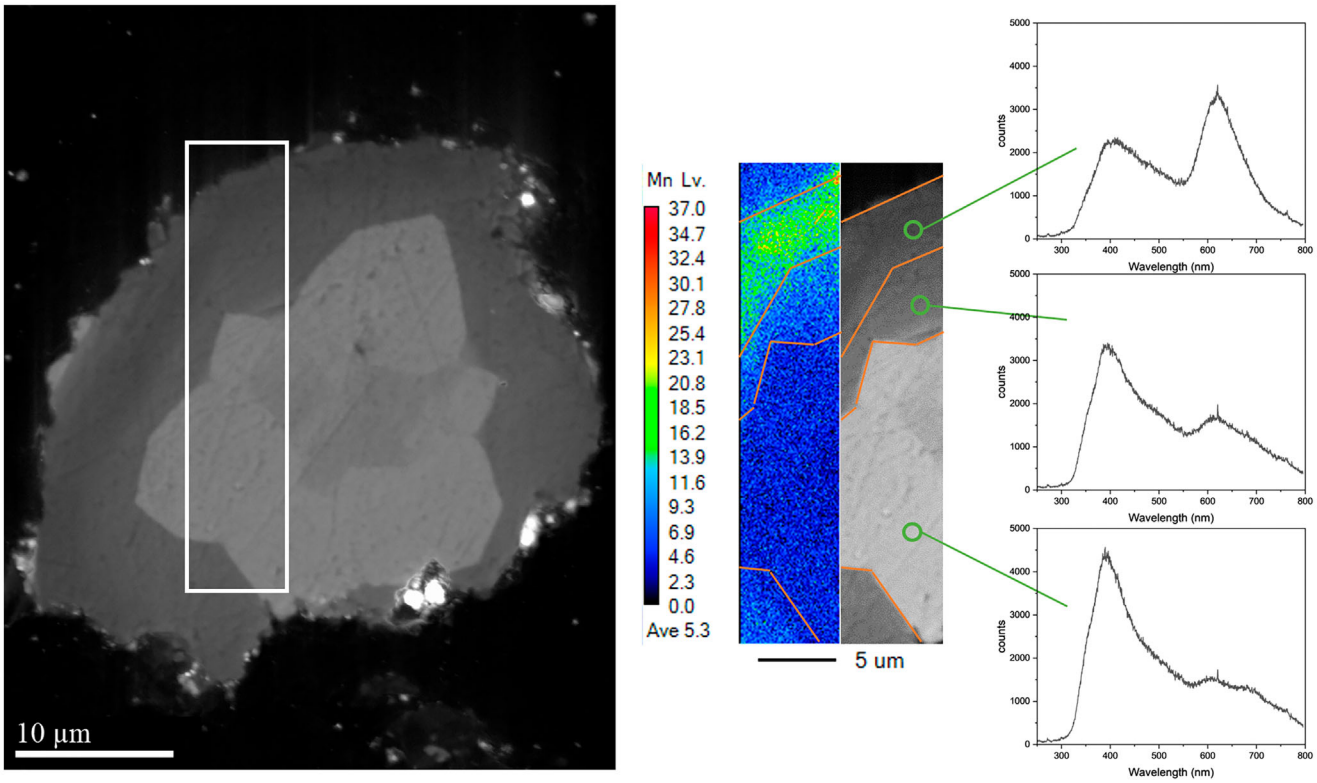

FIGURE 5. HR-CL panchromatic image of C4 calcite grain with corresponding CL spectral analyses compared with X-ray map of Mn obtained by EMPA. In this calcite, the highest content of MnO amounts to 0.51 wt%. Note that CL intensities in panchromatic images are not directly related to photons quantities due to a variation of sensibilities along visible light. The EPMA scale is in absolute intensity values.

in direct contact with the chondrite matrix (C1, C3, C71, C26–C29 in Figure S6 Supplementary Material). Fe-Ni sulfide crystals are also present in polycrystalline and microporous calcite aggregates (C26–C29 in Figure S6 Supplementary Material) which are like calcite grains of the T2 population.

Comparison between SEM-BSE and HR-CL images is also useful to establish whether there is a link between the internal CL zoning of calcite and the orientation of the hydrated polycrystalline (serpentine/tochilinite) phases. This is generally the case for calcites showing a marked core-edge CL zoning (Figure 5). In patches where calcite forms bands alternating with serpentine/tochilinite assemblage, HR-CL reveals instead that calcite is monocrystalline with no or at most poorly defined zoning (C101, C102 in Figure S6 Supplementary Material).

No particular trend emerges as well between internal CL calcite features and clasts. In most occurrences, the calcite is occupying the center of the serpentine/tochilinite patch, resembling a filled cavity. With this configuration, it is not clear whether the calcite formed by crystals growing toward the center of a pore from its margins or the reverse.

Spectral Analysis of Carbonates

From this inventory, an in-depth spectroscopic study has been undertaken to better characterize what is responsible for the distinct CL zoning in calcite. Panchromatic images described previously correspond, for a given scanned position, to the count integration of photons emitted at all the wavelength (over the sensitivity range of the detector, namely ~200/950 nm). For quantifying the spectral response of the carbonates, the panchromatic luminescence radiation coming from the scanned sample has been analyzed by directing it toward the monochromator of the CL setup (see experimental part).

Two main spectral luminescence centers characterize the carbonates of Cold Bokkeveld (Figures 5 and 6): an emission band in the range 375–425 (±10) nm (violet–blue), and for most of them, a second emission band peaking at 620 (±10) nm (orange). Both emissions show significant variations in their absolute and relative intensities. These two luminescence centers are generally interpreted in carbonates as resulting from intrinsic structural defects of the calcite lattice and extrinsic centers corresponding to Mn ion substitutions, respectively (see discussion). It is worth

19455100, 0, Downloaded from https://onlinelibrary.wiley.com/doi/10.1111/maps.14225 by Universite Cote D'azur, Wiley Online Library on [11/06/2024]. See the Terms and Conditions (https://onlinelibrary.wiley.com/terms-and-conditions) on Wiley Online Library for rules of use; OA articles are governed by the applicable Creative Commons License

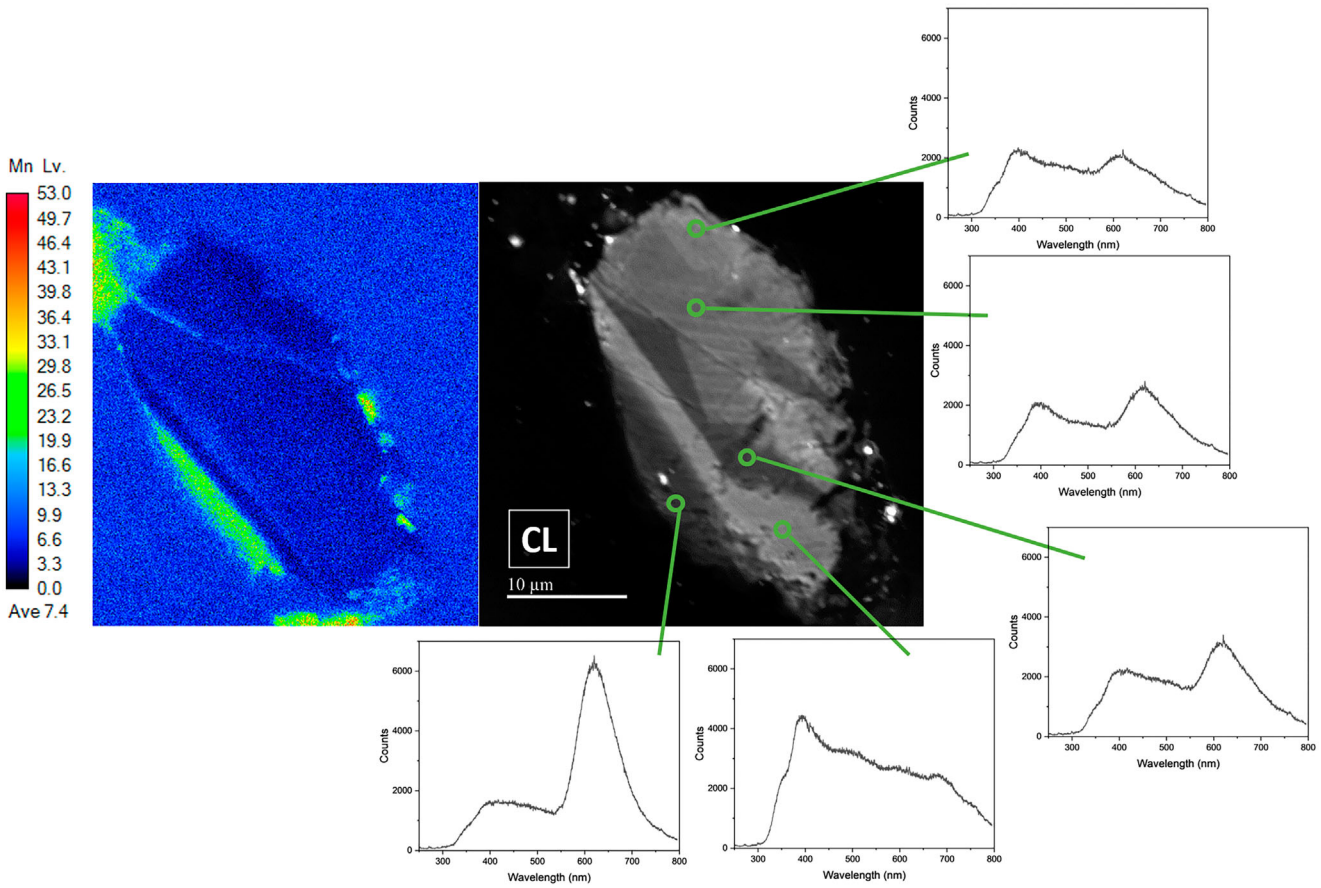

FIGURE 6. HR-CL panchromatic image of C5 calcite grain with corresponding CL spectral analyses compared with X-ray map of Mn obtained by EMPA. The maximum MnO concentration max = 0.51 wt%. Note that CL intensities in panchromatic images are not directly related to photon quantities due to a variation of sensibilities along visible light. The EPMA scale is in absolute intensity values.

mentioning that we do not have a direct quantitative correlation between the panchromatic HR-CL image and spectral analysis performed on a local point of the carbonate as both modes are performed using different detectors and light pathways (straight line + photomultiplier for panchromatic CL and grazing element + CCD for spectral analysis) which leads to different experimental response curves for each mode.

EMPA on representative carbonates (Table S1 and Figure S4) confirms the covariation of the 620 (±10) nm emission band intensity and the Mn concentration (e.g., Habermann et al., 1998) for T1 calcites and their absence for T2 ones. Whatever the clast analyzed (Table S1) and the internal zonation of the T1 calcite (Figures 5 and 6), we found that Mn is systematically enriched at each grain edge. Some calcite areas show variations in the orange peak that are not visible on the chemical map, which indicates the greater sensitivity of HR-CL by comparison with EMPA measurements to detect small Mn variations in the range of 10–100 ppm.

Having identified the main spectral response of the analyzed object in spectral mode, filtered panchromatic imaging can be done using bandpass filters (Figure 7). Centered bandpass filters 400 (±20) nm and 620 (±10) nm have been used here to better map areas dominated by intrinsic structural defects and those dominated by Mn^{2+} content within the same calcite crystal, respectively (Figure 7). In this configuration, one can see that sharp CL zonation in T1 calcites are mainly due to structural defects promoting a strong intrinsic luminescence whereas Mn variations in the lattice promote a more variable extrinsic luminescence (Figure 7). These quasi-monochromatic images also confirm the concentrically zoning of the carbonate with preferential enrichment of Mn at calcite edge and its depletion in the center. Finally, it is worth noticing that the Mn emission centers responsible for the 620 nm photons have a long-life expectancy, related to phosphorescence mechanism (ms scale), faster than the scan rate of FEG-SEM, inducing comet tail-like artifacts on CL images.

19455100, 0, Downloaded from https://onlinelibrary.wiley.com/doi/10.1111/maps.14225 by Universite Cote D'azur, Wiley Online Library on [11/06/2024]. See the Terms and Conditions (https://onlinelibrary.wiley.com/terms-and-conditions) on Wiley Online Library for rules of use; OA articles are governed by the applicable Creative Commons License

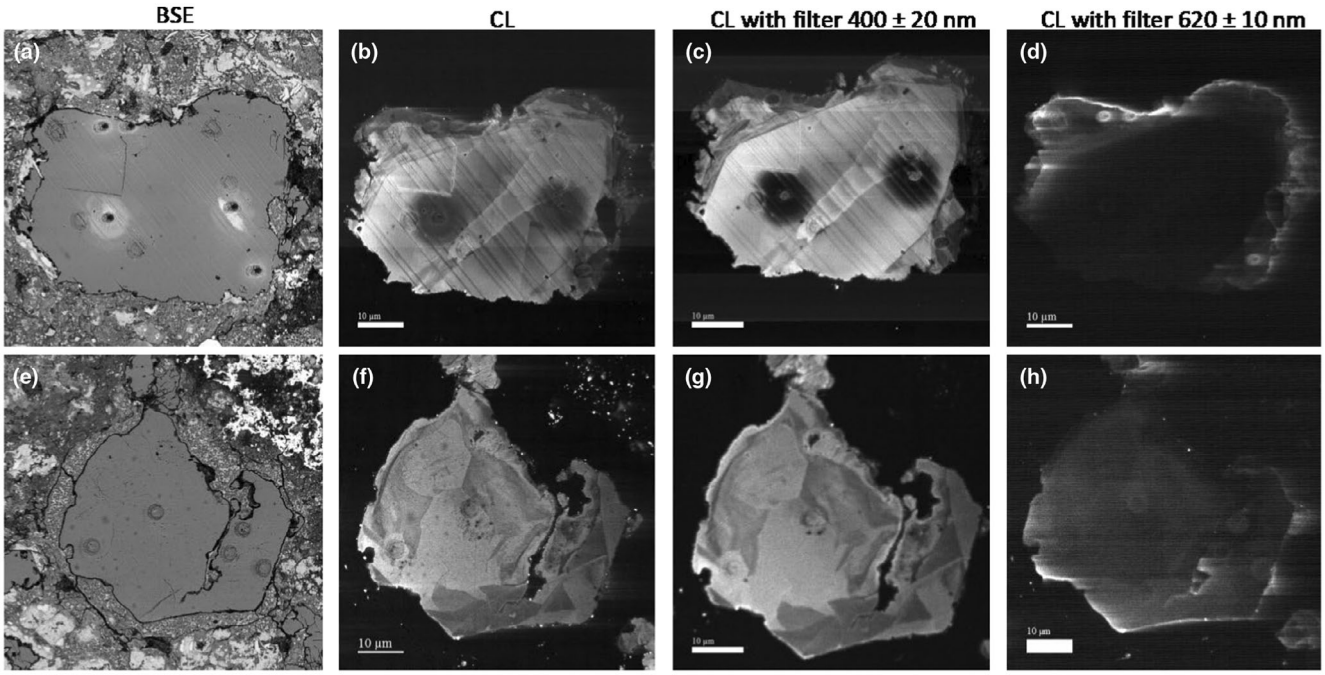

FIGURE 7. BSE (a and e) and HR-CL panchromatic images (b and f) of C18 and C15 calcite grains combined with filtered images at 400 (±20) nm (c and g) and 620 (±10) nm (d and h) wavelength, respectively. These filters help to separate contributions from photons with a wavelength of 400 nm, attributed to intrinsic structural defects, and those dominated by Mn^{2+} concentration, associated with the 620 nm photons. Notice the comet tail-like artifacts on images d and h, due to the phosphorescent effect of long-life expectancy photons from Mn emission centers. The photons emitted on the borders of grains can be associated with grain boundary artifacts.

Spectral line scans can also be acquired across T1 or T2 calcites to document the CL variations inside each individual grain (Figure 8). They show the clear spectral difference existing between the two populations of calcites from Cold Bokkeveld consistent with EMPA analyses (Table S1 and Figure S4). T1 calcites are on average characterized by a variable intensity of the orange wavelength domain. T1 grains are frequently (concentrically) zoned showing cores dominated by blue emissions and edges by orange ones. This contrast with the more homogeneous CL of T2 calcites, characterized by a higher contribution of the blue domain and less pronounced variation around the orange emission.

DISCUSSION

Carbonates in CM Carbonaceous Chondrites

Carbonates in CM carbonaceous chondrites received a lot of attention in the last decades, as they represent direct proxies of the hydrothermal activity of their parent body in which they formed and can, in theory, be used to decipher their thermal evolution (Alexander et al., 2015; Clayton & Mayeda, 1984; Clog et al., 2024; Guo & Eiler, 2007; Verdier-Paoletti et al., 2017). Several attempts have thus been made to correlate the extent of alteration to the properties of the fluid as recorded mainly by the oxygen isotopic composition of carbonates (Lee et al., 2013; Lindgren et al., 2017; Riciputi et al., 1994; Tyra et al., 2012, 2016; Vacher et al., 2017, Vacher, Piralla, et al., 2019; Verdier-Paoletti et al., 2017; Suttle et al., 2021). A consensus emerges around the fact that calcite precipitated from the fluid phase, initially infilling void space, forming vugs, and/or acting as a cement in CM parent bodies. Early alteration produced Fe-bearing calcite while later alteration favored the precipitation of Mg-bearing calcite (e.g., Lee et al., 2013; McSween et al., 2018; Rubin et al., 2007). The minor element cation compositions of calcite, therefore, mirror the evolution trend observed in phyllosilicates, further demonstrating that secondary phase compositions are directly related to the composition of the alteration fluid, both in terms of their chemistry (Velbel et al., 2012, 2015) and isotopic composition (Lindgren et al., 2017).

In more detail, petrographic and isotopic approaches have revealed that T1 calcites formed before the main growth windows for phyllosilicate and sulfides. These early calcites may have coprecipitated with other complex carbonates (e.g., breunnerite) facilitated by the presence of increasingly Mg-rich solutions (Lee et al., 2012). It is also inferred that T1 calcites precipitated at lower temperatures

19455100, 0, Downloaded from https://onlinelibrary.wiley.com/doi/10.1111/maps.14225 by Universite Cote D'azur, Wiley Online Library on [11/06/2024]. See the Terms and Conditions (https://onlinelibrary.wiley.com/terms-and-conditions) on Wiley Online Library for rules of use; OA articles are governed by the applicable Creative Commons License

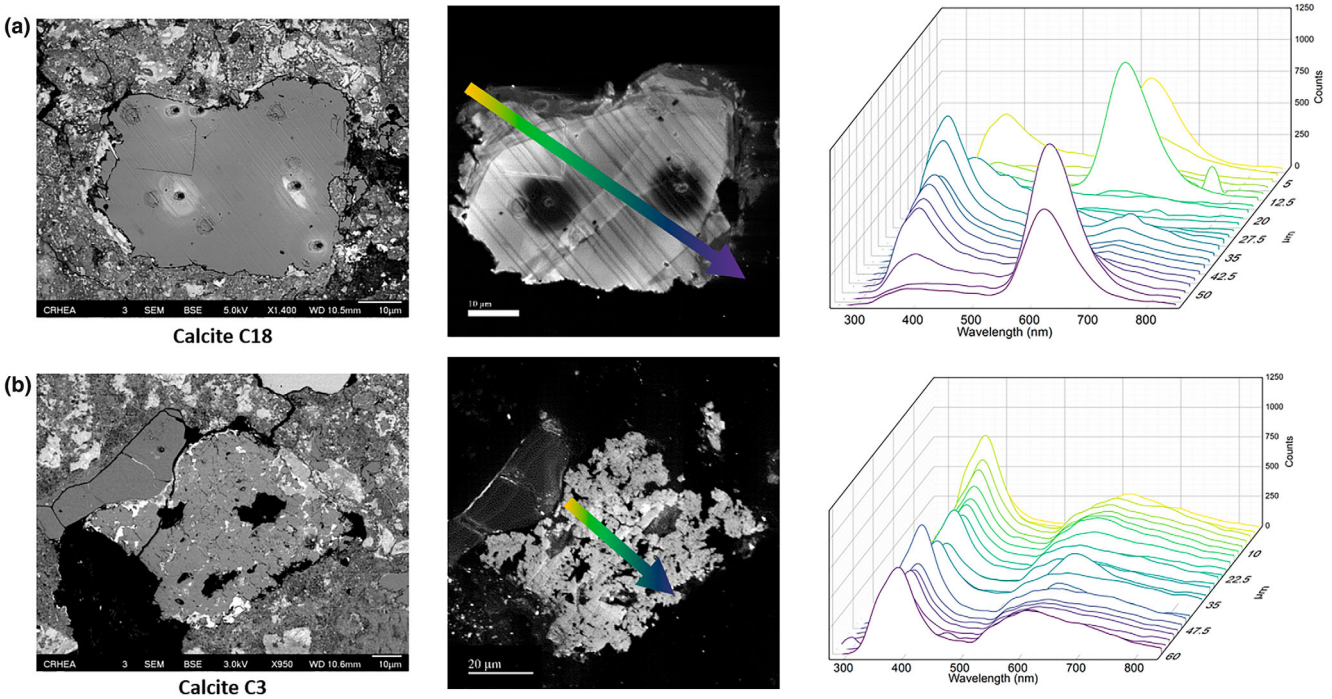

FIGURE 8. BSE (left row) and HR-CL panchromatic images (middle row) with spectral line scans (right row) acquired across representative T1 (a, C18 grain) or T2 (b, C3 grain) calcites, along the arrows, showing the dichotomy in luminescence existing between these two populations of calcites from the Cold Bokkeveld CM2 chondrite. Grading colors in the spectral line scans is an indicator of where the spectra were acquired with the corresponding colors of the arrows on the panchromatic images.

than serpentines and T2 calcites. This implies that fluid circulation in CM parent bodies, and thus the formation of CM secondary phases, occurred during a prograde thermal evolution (e.g., Lee et al., 2013; Farsang et al., 2021; Suttle et al., 2021; Vacher, Piralla, et al., 2019), with T1 calcites forming first at low temperature (<50°C), followed by the precipitation of (Fe,S)-rich serpentine and tochilinite at intermediate temperature (30–100°C), and finally T2 calcites at temperature circa 110–245°C. This inferred prograde thermal path (increasing temperatures with time), concurrent with a decreasing W/R ratio as water was progressively consumed in hydration reactions (Rosenberg et al., 2001).

In such prograde alteration occurring under variable water-to-rock ratio (Clog et al., 2024; Suttle et al., 2021; Vacher, Piralla, et al., 2019), two main generations of calcite are inferred: a low temperature first-generation T1 calcites and a higher temperature second-generation T2 calcites.

Carbonates Distribution in the Cold Bokkveld Chondrite

A visual inspection of X-ray chemical maps of the chondrite (Figures 2, 3 and S2, S3) reveals that 2-D calcite grains spacing or density seem relatively constant within each clast or in the matrix (Rubin et al., 2007), but do vary significantly from clast to clast. This configuration is interesting because it raises the question of whether these density heterogeneities of calcites are inherited from the evolution specific to each clast prior to the chondrite accretion/formation. This is all the more legitimate as each clast in Cold Bokkeveld shows a different degree of alteration between 2.1 and 2.7 according to Lentfort et al. (2020). The Fe/Si ratio X-ray chemical map (supplementary material), however, suggests that carbonate crystallization is independent of the clasts' alteration degree, corroborating previous findings (De Leuw et al., 2010; Farsang et al., 2021; Lee et al., 2013; Lentfort et al., 2020; Sofe, 2013). That said, the problem remains with no explanation about why calcite abundance is unrelated to the degree of alteration. A dedicated study should be conducted on the relationship between the nature and abundance of carbonate phases and the degree of alteration of the clasts containing them.

The Unique Message of HR-CL on Carbonates

Compared to terrestrial carbonates, only a few studies have used CL to characterize carbonates in chondrites and only a handful have been focused in calcite (Brearley & Hutcheon, 2002; Farsang et al., 2021; Fujiya et al., 2020; Lee et al., 2014; Lee & Ellen, 2008; Telus et al., 2019). In these studies, the CL

19455100, 0, Downloaded from https://onlinelibrary.wiley.com/doi/10.1111/maps.14225 by Universite Cote D'azur, Wiley Online Library on [11/06/2024]. See the Terms and Conditions (https://onlinelibrary.wiley.com/terms-and-conditions) on Wiley Online Library for rules of use; OA articles are governed by the applicable Creative Commons License

was mainly used to provide CL panchromatic images of calcite grains or to make the difference between Mn-poor (those with 620 nm peaks with low counts) from Mn-rich (those with 620 nm peaks with high counts) calcite since CL in calcite is predominately activated by Mn^{2+} impurities in the crystal lattice. It is important to notice, however, that the two populations of Mn-poor and Mn-rich calcites in MET 01070 CM chondrite distinguished by Telus et al. (2019) belong to the T1 calcites, since as noticed by the authors, Mn-rich calcite grains are anhedral and often occur along the periphery of euhedral/subhedral Mn-poor calcite grains.

The high sensitivity of HR-CL to subtle changes in the chemistry or the structure of the crystal allows panchromatic CL images to give a unique and prompt insight on carbonates precipitated in chondrite matrices, here calcite. As revealed by changes in the intensity of the panchromatic images, HR-CL reveals zoning which in turn may give us access to the mode of growth of the calcite into the porosity of the matrix. The present survey (Figures 4–8 and S6 Supplementary Material) shows different morphologies of calcite: single grain, polycrystalline and/or porous aggregate, intergrowth with serpentine/tochilinite assemblage, with homogenous, concentric, or blurred chemical zonings. Despite a significant number of CL analyses, it is difficult to establish whether one type of grain and morphology dominates on the others in the whole sample or from clast to clast. The only obvious difference concerns the panchromatic CL images between T1 and T2 grains trend, with the former showing more complex zoning than the latter. Panchromatic CL images of T1 grains, like C4, C5, C18, C19, C21, and C51, show indeed remarkable concentric zoning with clear epitaxial overgrowth episodes suggestive of some changes in fluid compositions or conditions during the precipitation of these calcites. T1 grains, like C14 and C15, show in contrast more complex and blurred zoning of growth and dissolution that could be interpreted as resulting from changes in the carbonate saturation of the fluid that precipitated them. Those grains could be opposed to other T1 grains, like C20, C65, C74, and C110, showing more homogeneous panchromatic CL images likely due to more quiescent growth conditions for these calcites, some of which being constituted of polycrystalline aggregates (e.g., C20, C34). Even if more work needs to be done, this shows already the potential of HR-CL panchromatic images in revealing key information about the carbonate growth mode, notably the main difference between T1 and T2 calcites (see below).

The CL spectral analysis of Cold Bokkeveld calcites (Figures 5–9) allows to go further, since two types of emission centers have been distinguished: a blue emission band (≈375–425 nm) linked to intrinsic structural defects and an orange extrinsic emission at lower energy (≈620 ± 10 nm) in response to Ca-Mn ion substitution (Habermann et al., 1998; Lee & Ellen, 2008). Spectral CL analysis consists of counts of photon for each wavelength analyzed and offers the possibility of characterizing the extrinsic and intrinsic CL contributions in calcite, separately, even if the precise relationships between luminescence intensities and absolute concentrations of ions and defects are still a matter of debate (Budd et al., 2000; Lee et al., 2005; Pagel et al., 2000; Toffolo et al., 2019). When the wavelength axis (nm) is converted in energy (eV), the plot can be deconvoluted in Gaussian peaks associated with different emission centers of the structure, as shown for the C15 calcite grain (e.g., Figures 9 and S5 in Supplementary Material). Each spectrum was thus fitted using five peaks, similarly as previous reports with fitted CL spectra on carbonates (Chapoulie et al., 2005; Garcia-Guinea et al., 2011; Toffolo et al., 2019). The three peaks in the range of 2.5–4 eV are usually associated with intrinsic defects of calcite, possibly induced by lattice distortions, anion vacancies or electron–hole recombination with $(CO^3)^-$ as electron and Ca^+ as hole. The two remaining peaks between 2 and 1.5 eV are associated with the substitution of Mn^{2+} for Ca^{2+} in the $CaCO_3$ lattice (Calderón et al., 1984; Habermann et al., 1998; Pagel et al., 2000; Toffolo et al., 2019).

The deconvoluted area of the main orange peak at 2 eV can be thus plotted (Figure 10) against the Mn concentration measured at the same location in the calcite grain by EMPA (Table S1). The difference between T1 and T2 calcites is obvious since no correlation is observed for T2 grains. On the other hand, a positive linear correlation exits for T1 confirming the major role of the Mn abundance on the extrinsic luminescence (Figure 10). Even if the curve fit remains rather broad, a good confidence can be however placed in this trend since it applies to both variations within the same T1 calcite grain and from grain to grain belonging to several clasts of Cold Bokkeveld chondrite. From this trend, several points need to be outlined. Mn concentrations in both T1 and T2 calcites in the range of several hundreds to thousands of ppm are sufficient to produce visually a detectable luminescence. This is consistent with the fact that Mn^{2+} concentration as low as 10–20 ppm is enough to activate the luminescence in carbonates (Machel, 2000). As already suggested, T1 calcites show highly variable luminescence intensities in the orange domain marked by a prominent increase at the grain edge, due to Mn enrichment as high as $\approx 10^4$ ppm (Figure 10; Table S1). This contrast with lower intensity of the orange peak and the lower Mn concentration measured in T2 calcites (Table S1; Figures 8 and 10). Not much data have been previously published concerning the Mn content in T2 calcites. Lee et al. (2013) looked at T2 calcites in a vein and matrix

19455100, 0, Downloaded from https://onlinelibrary.wiley.com/doi/10.1111/maps.14225 by Universite Cote D'azur, Wiley Online Library on [11/06/2024]. See the Terms and Conditions (https://onlinelibrary.wiley.com/terms-and-conditions) on Wiley Online Library for rules of use; OA articles are governed by the applicable Creative Commons License

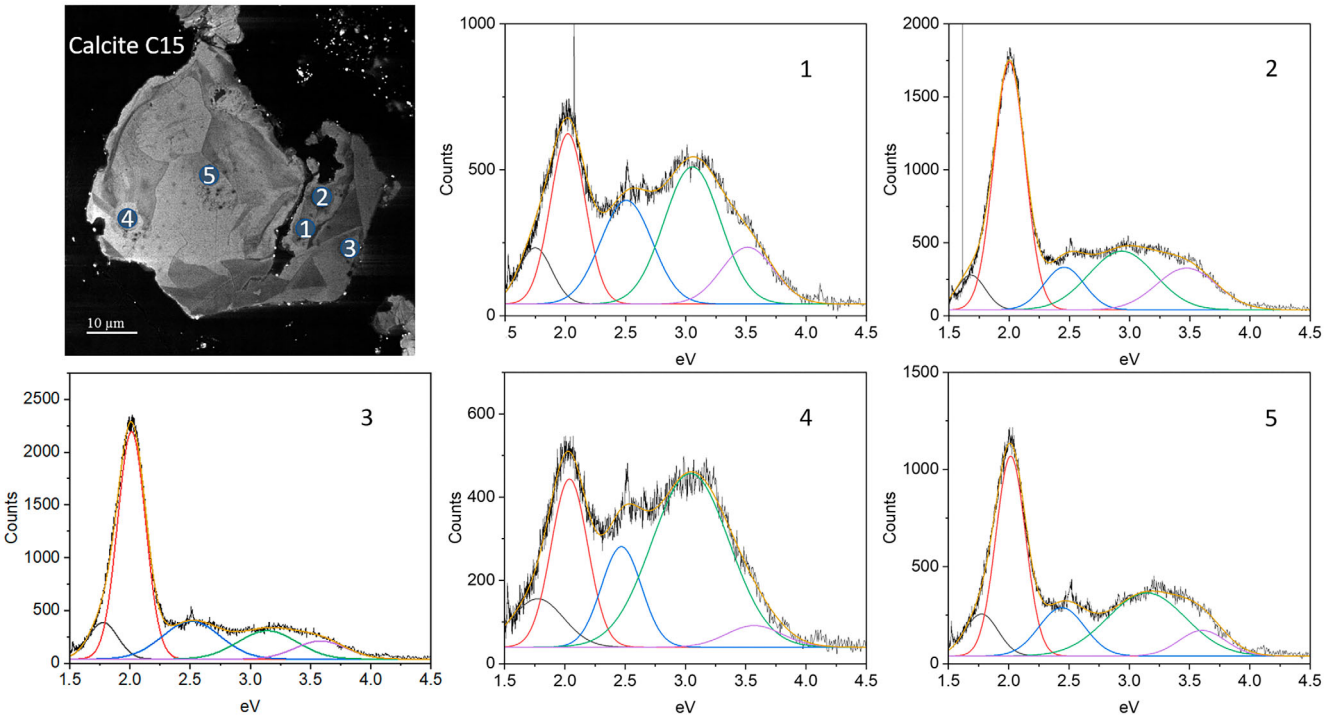

FIGURE 9. Deconvolution of HR-CL spectra (CL peaks fitting) of C15 calcite grain, using three peaks in the range of 2.5–4 eV usually associated with intrinsic defects of calcite and two peaks in the range 2–1.5 eV associated with the substitution of Ca^{2+} for Mn^{2+} in the $CaCO_3$ lattice. See text.

grains in LON 94101 CM chondrite and found Mn to be below EPMA detection limits. Tyra et al. (2012) did get measurable Mn in T2 calcites in two EET 96016 and EET 96006 CM2 chondrites and find that Mn is present low concentrations in T2 calcites in the range of ≈1000 ppm or lower. The 2 eV peak area measured for T2 calcites also confirms that T2 calcites are less enriched in Mn and more homogeneous than T1 grains (Figures 8 and 10). They differ, however, from the low Mn T1 calcite cores by their higher intensity of the higher 2.5–4 eV energy bands. On average, T2 calcites have blue bands twice as intense as those the low Mn T1 calcite cores.

Because compositionally pure calcite luminesces at blue wavelengths, this emission is believed to be related to intrinsic sites of the calcite crystal such as Ca^{2+} and CO^{3-} sites (Calderón et al., 1984). However, the present study shows that the blue emission is more complex and possibly a composite of different energy levels, including lattice distortions which could modulate the existing energy emission or enabling new radiative recombination transitions. This may be indicated by the peak fitting (Figures 9 and S5 in Supplementary Material), which shows that the main blue emission masks other minor emissions at specific energy levels. These may represent other structural defects that are currently unknown, especially distortions in the crystal lattice caused by heat and/or rapid precipitation of $CaCO_3$ crystals. Another concern is whether variations of intrinsic blue peak intensity are somehow related to the presence or absence of network defects related to the substitution of trace elements in calcite (e.g., Ca^{2+} for Mn^{2+}). A better understanding of how intrinsic luminescence is generated and its significance in terms of calcite formation conditions requires a more dedicated study with suitable calibration using other methods, an objective clearly beyond the scope of this paper. Nevertheless, HR-CL at this stage already provides evidence of a dichotomy between T1 (with CL varying from dull to bright) and T2 (dull CL) calcites grains, differing not only by their chemistry but also by their lattice defects.

It is informative that the oxygen isotope composition of calcites in CM chondrites, including Cold Bokkeveld chondrite, follows the same trend (Farsang et al., 2021; Fujiya et al., 2015, 2020; Lee et al., 2013; Telus et al., 2019; Tyra et al., 2012; Vacher et al., 2017). Vacher, Piralla, et al., 2019 show, for instance, that the O isotopic compositions of T1 calcite grains measured vary widely, with $\delta^{18}O$ values ranging from 23.1 to 44.3‰, $\delta^{17}O$ from 11.1 to 23.4‰, and $\Delta^{17}O$ from −2.8 to +1.8‰, whereas T2 calcite grains have homogeneous compositions with $\delta^{18}O$ values ranging from 12.6 to 18.4‰, $\delta^{17}O$ from 4.2 to 8.1‰, and $\Delta^{17}O$ from −4 to −0.8‰. As for the CL data, the clear oxygen isotope dichotomy, with T1 grains isotopically heavier and more heterogeneous than the T2 ones, may be consistent with formation under dissimilar fluid compositions and conditions.

19455100, 0, Downloaded from https://onlinelibrary.wiley.com/doi/10.1111/maps.14225 by Universite Cote D'azur, Wiley Online Library on [11/06/2024]. See the Terms and Conditions (https://onlinelibrary.wiley.com/terms-and-conditions) on Wiley Online Library for rules of use; OA articles are governed by the applicable Creative Commons License

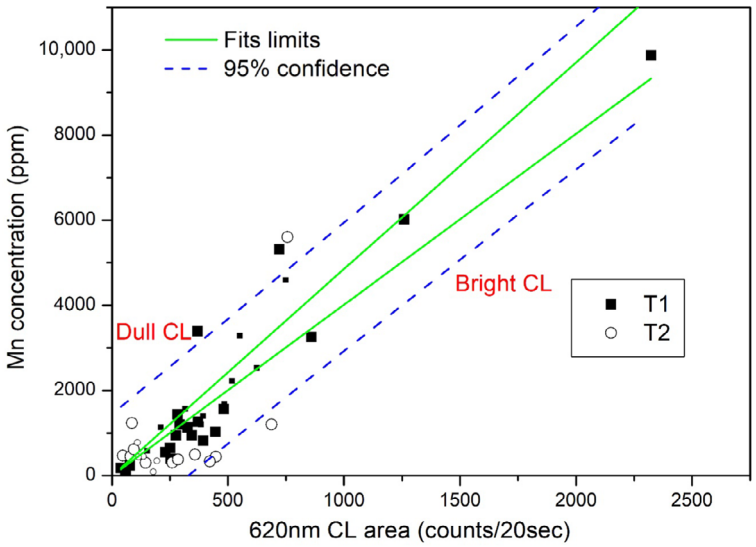

FIGURE 10. Deconvoluted area of the main orange peak at 2 eV plotted against Mn concentration measured by EMPA at the same location in various calcite grains from the Cold Bokkeveld CM2 chondrite. Notice the difference between T1 (square) and T2 (circle) calcites. Only T1 calcites (large square) obeying to the stoichiometry are fitted: $Mn_{T1Calcite}$ in ppm = 4.4 × Area 620 nm peak in counts/20s, R^2 = 0.94. Notice that the EMPA detection limit for Mn is around 250–300 ppm. The positive linear correlation confirms the major role of the Mn abundance on the extrinsic luminescence in T1 calcite (see text for discussion and supplementary material).

HR-CL Contribution to Constraining Carbonate Formation in CM Chondrites

In response to our introductive questioning, we show in the following how CL emission can be used to detect activator elements, their variations, and help to shed light on the mode/condition of formation of calcite in CM chondrites. This assumes that concentrations of trace elements in solids (e.g., Mn in calcite in the context of this study) are governed by the ratio of the activities of Ca^{2+} and Mn^{2+} ion in the aqueous solution from which they equilibrate $(aMn^{2+}/aCa^{2+})_{fluid}$ rather than by the absolute cation activities or concentrations in aqueous solution.

This CL study confirms the existence of two different populations of calcite grains. In addition, it shows that each population has their own characteristics (variability of Mn contents and lattice defects) that correlates with different textural environments. The T1 calcites, characterized by variable CL and peripheral Mn enrichments, are always mantled by a rim composed of Fe-S rich serpentine–tochilinite assemblage, while T2 calcites characterized by homogeneous CL and higher lattice defect are in direct contact with the matrix. They are serpentine-free polycrystalline aggregates of calcite grains, containing Fe-Ni sulfide inclusions, and in direct contact with the matrix.

Even though a quencher of Mn^{2+}-activated luminescence in calcite is Fe^{2+}, the interplay of Mn^{2+} and total Fe (i.e., Fe^{2+}+Fe^{3+}) in determining the luminescence characteristics of natural carbonates is not well understood. In general, the Fe^{2+}/Mn^{2+} ratio exerts a control on the intensity of carbonate luminescence (Machel, 2000). Nevertheless, the lack of any correlation between Mn and Fe in calcite from Cold Bokkeveld (Table S1 and Figure 10) implies that the absolute concentrations of Mn^{2+} alone are more likely to be the primary parameter determining the intensity of the observed luminescence and its variability, ranging from dull to bright. This observation was made as we examined the carbonate grains from core to rim in T1 or potentially in T2 (Figure 8; also refer to Machel, 2000). The relatively constant Fe content in calcites (approximately ≈1 wt% FeO; Table S1 and De Leuw et al., 2010) suggests that the iron concentration in the fluid phase was potentially regulated by the co-precipitation of iron-bearing phases. For instance, in the case of T1 calcites, this may involve the co-precipitation of iron-bearing phases such as Fe-S-rich serpentine/tochilinite, while in the case of T2 calcites, the co-precipitation of iron–sulfide could play a role.

On this basis, changes in the orange CL emission intensity of calcites can also be interpreted in the light of changes in redox-potential (Eh) in the fluid phase, since these changes affect concentrations of elements which have different valence states, including Fe and Mn and the partitioning of these elements in precipitated phases. As with iron, manganese aqueous geochemistry is governed by oxidation and reduction, which is conveniently displayed using Eh-pH diagrams (Barnaby & Rimstidt, 2014; Force & Maynard, 1991; Maynard, 2003). Figure 11 shows the stability fields of

19455100, 0, Downloaded from https://onlinelibrary.wiley.com/doi/10.1111/maps.14225 by Universite Cote D'azur, Wiley Online Library on [11/06/2024]. See the Terms and Conditions (https://onlinelibrary.wiley.com/terms-and-conditions) on Wiley Online Library for rules of use; OA articles are governed by the applicable Creative Commons License

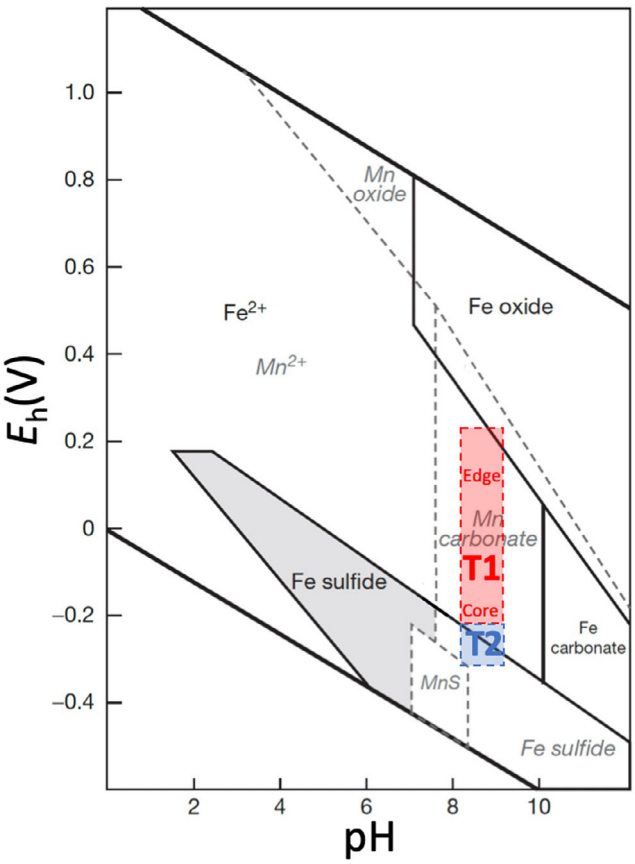

FIGURE 11. Superimposed Eh-pH diagrams of manganese (dashed lines) and iron species (plain lines), modified from Maynard 2014. Note the relatively large field of stability of dissolved Mn^{2+} as well as the large field of stability for Fe sulfide compared to manganese sulfide under reducing conditions. Expected stability field of T2 and T1 calcites under reducing and moderately reducing conditions, respectively, together with indication of their CL intensity (non, dull, or bright). Note that Eh-pH ranges for T1 and T2 calcites are only indicative. See text for discussion.

the most common manganese/iron oxides and carbonates as a function of Eh and pH. Dissolved manganese has a relatively large field of stability as Mn^{2+}. At pH values, commonly found on Earth in surface waters, 5–7 for freshwater and 8 for seawater, manganese is relatively soluble under mildly to strongly reducing conditions. The addition of carbonate species to the system creates a large region in which condensed manganese, in the form of the carbonate rhodochrosite ($MnCO_3$), is stable under reducing conditions. Adding sulfur to the system does not significantly change this picture. Unlike iron, which forms insoluble sulfides, manganese has a soluble sulfide (MnS, alabandite). Therefore, under reducing conditions, the solubility of manganese is primarily regulated by carbonate minerals, whereas iron solubility is predominantly influenced by sulfides (Maynard, 2003).

Interestingly, such Eh-pH relationship suggests a mechanism for separating manganese from iron. Figure 11 shows that soluble manganese has a considerably larger stability field than soluble iron under moderately reducing conditions. In these conditions, Mn^{2+} is commonly mobilized into the pore water, while iron remains fixed as an oxide or hydroxide. Under conditions of low Eh and high sulfur content, such as in reducing conditions, the iron is fixed as a sulfide, but manganese is still mobile. Dissolved Mn^{2+} concentrations in the pore waters may be then free to partition into calcite according to the ($a Mn^{2+}/a Ca^{2+}$) ratio of the fluid phase (see above).

Following the above reasoning, T2 calcites and their associated Fe-Ni sulfide inclusions may have been precipitated from reducing and alkaline solutions (e.g., enriched in HCO_3^-, CO_3^{-2}, and OH^- ions) in which dissolved Mn^{2+} concentrations in the pore waters is low and iron sulfides are stable phases (Figure 11). In contrast, T1 calcites seem to precipitate from a different fluid under moderately reducing conditions in which Mn^{2+} is soluble and variable, explaining their CL oscillatory zoning and/or core to edge CL variations. Such inferred higher oxidation conditions for T1 calcites are also consistent with their close association with magnetite (e.g., Farsang et al., 2021), the high $Fe^{3+}/\Sigma Fe$ ratio measured in Fe-rich tochilinite (e.g., Pignatelli et al., 2017), and the general lack of associated iron sulfides (e.g., De Leuw et al., 2010; Lee et al., 2014).

As shown by Dromgoole and Walter (1990) on their experimental study on iron and manganese incorporation into calcite, effects of precipitation rate and temperature on DMn^{2+} and DFe^{2+} could produce marginal compositional variations in calcite causing cathodoluminescence zoning but are unlikely to be responsible for the major variations commonly observed in natural calcite. Instead, they show that changing redox conditions are responsible for the CL zoning in calcite since most major luminescence transitions are accompanied by an increase in the concentration of Mn (brighter) while the concentration of the other metal remains nearly the same or decreases (see Table S1 and Figure 9). Applied to CM chondrites, this may question the isotopic models invoking a gradual increase in temperature up to 250°C during a prograde evolution, that is, T2 calcites and serpentine precipitated at higher temperatures than T1 calcites (Clog et al., 2024; Lee et al., 2014; Suttle et al., 2021; Vacher, Piralla, et al., 2019).

Such a prograde evolution of CM parent bodies also raises questions concerning the thermal destabilization of the hydrous phases already precipitated (e.g., TCIs). Tochilinite is the most thermally sensitive mineral in CM chondrites. Estimates of its breakdown temperature range from 120°C (Zolensky et al., 1997) to 245°C (Fuchs et al., 1973) and 300–400°C (Nozaki et al., 2006). Similarly, recent heating experiments (Garenne

19455100, 0, Downloaded from https://onlinelibrary.wiley.com/doi/10.1111/maps.14225 by Universite Cote D'azur, Wiley Online Library on [11/06/2024]. See the Terms and Conditions (https://onlinelibrary.wiley.com/terms-and-conditions) on Wiley Online Library for rules of use; OA articles are governed by the applicable Creative Commons License

et al., 2014; King et al., 2021; Libourel et al., 2021; Lindgren et al., 2020) on CM chondrites have shown that significant mass loss events, attributed to dehydration or the beginning of dehydroxylation (release of H_2O and OH) of phyllosilicates and Fe-(oxy-) hydroxides, occurred at temperature circa or slightly below 300–400°C.

Assuming that the various alteration degrees in clasts have been acquired in their respective parent body, the presence of several distinct types of clasts indicates a complex mixing in a dynamic environment and involving material from various sources (see Lindgren et al., 2013 amongst other). In this scenario, the various degrees of alteration of individual clasts constituting the present CM breccia could give insights on the permeability and/or the heterogeneity of the hydrothermal system responsible of the alteration of the "sampled" parent body. Without chronological constraints, another alternative would be that some of these clasts would come from different parent bodies of different ages and at different level of alteration.

The chemical composition of the fluid responsible of the ubiquitous precipitation of serpentine/tochilinite assemblages and T1 calcites in pores has probably evolved at low water/rock ratio in closed system from one pore to another to account for CL zoning in T1 calcites (oscillatory or heterogeneous) and variable modal abundance of precipitates in each pore (serpentine/tochilinite/calcite). Similarly, the variable modal abundance of T1 calcite in the various clasts and the matrix (Figures 2, 3 and supplementary material) hints for local variations of the $aCa_{(fluid)}$ calcium activity of the fluid and its alkalinity hosted in micro-porous environments. In this respect, it might be interesting to evaluate whether calcite modal proportion in clasts is proportional to their bulk calcium content or the high modal abundance of Ca-bearing phases, for example, pyroxenes, from chondrules or refractory inclusions. The relative homogeneity of CL intensity in the rare T2 calcites (low Mn and high intrinsic CL) as well as the relative homogeneity of the "FeO"/SiO_2 ratio of TCIs in each individual clast (Lentfort et al., 2020) suggest large-scale aqueous alteration in an open system and lower redox conditions (Figure 11).

It has been shown that the Mg content of serpentine increases with increasing overall degree of aqueous alteration, so CM2 chondrites with Mg-rich serpentines experienced a more advanced degree of aqueous alteration than CM2 chondrites with Fe-rich serpentines (Lentfort et al., 2020; Leroux et al., 2015; Rubin et al., 2007; Velbel & Palmer, 2011). This composition is probably the consequence of the preferential dissolution of metal and iron sulfides during the first stages of alteration. In this case, both episodes of alteration responsible of T1 and T2 calcites in Cold Bokkeveld/CM chondrite parent body seem to proceed in the same way with the same precipitation sequence: Fe-rich serpentines/S-bearing phases (sulfides or tochilinites)/calcite, from a fluid acting (i) at different scale, (ii) different Eh-pH conditions, and (iv) having different oxygen isotope compositions (Clog et al., 2024; Tyra et al., 2012; Vacher, Truche, et al., 2019).

Because of these trends, we thus suggest that terrestrial serpentinization of basaltic and ultramafic rocks that have relatively low silica contents (45%–52% and <45%, respectively) but a high content of ferromagnesian minerals like olivine and pyroxene is a valuable proxy of the aqueous alteration taking place on CM chondrites; a comparison that deserves to be studied in more detail. Alteration of these minerals in contact with water during free hydrothermal circulation leads to "serpentinization," a process in which olivine/pyroxene reacts with water. This may lead to the formation of serpentine, magnetite, brucite, and molecular hydrogen (Barnes et al., 2009; Mevel, 2003; Roumejon et al., 2018; Seyfried et al., 2007 amongst other). The process may also be associated with increasing alkalinity which promotes low-temperature carbonatation in the hydrothermal fluid favoring the precipitation of several calcite generations crosscutting the serpentine mesh textures (Frue-Green et al., 2004; Mevel, 2003; Picazo et al., 2020; Russell et al., 2005; Scicchitano et al., 2022). As in CM chondrites, it has been shown that CL of calcite is activated by Mn^{2+}, whose emission color is orange (Picazo et al., 2020) and that temperature is not strongly influencing the Mn uptake in calcite grains. It is also suggested that the Eh-dependent solubility of Mn into the fluid might allow using CL color variations as a proxy for oxygen fugacity variations in the fluid (Picazo et al., 2020).

Serpentinization followed by carbonatation is, however, a retrograde process in ocean floor serpentinites (Bach et al., 2006; Mevel, 2003), in contrast to the actual consensus around a prograde thermal evolution during the aqueous alteration in CM chondrites (Clog et al., 2024; Suttle et al., 2021 among some recent contributions). More work clearly needs to be done to solve this issue, for instance by using HR-CL as a pre-screening tool for secondary-ion mass spectrometry (SIMS) oxygen isotope analyses, as it has been done by Fujiya et al. (2015, 2020), to characterize the core-edge O-isotope variations of calcites from CM2 chondrites with low (e.g., Asuka 12169,81; Kimura et al., 2020), intermediate (e.g., Cold Bokkeveld) to high degree of alteration (e.g., Winchcombe CM2 fall; Greenwood et al., 2023; Suttle et al., 2023). Supplemented by Mn-Cr ages of carbonates (Fujiya et al., 2012), these results will be of fundamental importance to shed light on thermal condition, mode, and timing of accretion of CM chondrite parent bodies and to

19455100, 0, Downloaded from https://onlinelibrary.wiley.com/doi/10.1111/maps.14225 by Universite Cote D'azur, Wiley Online Library on [11/06/2024]. See the Terms and Conditions (https://onlinelibrary.wiley.com/terms-and-conditions) on Wiley Online Library for rules of use; OA articles are governed by the applicable Creative Commons License

ascertain if the primary driver of aqueous alteration was ^{26}Al radiogenic decay (Doyle et al., 2015).

CONCLUSIONS

As it has been outlined in numerous previous studies, carbonate minerals in the CM carbonaceous chondrites provide a wealth of insights into the evolution of parent body porosity and permeability, water/rock ratio, and the longevity and chemistry of aqueous solutions (Lee et al., 2014). To participate to this endeavor and to make the best use of it to understand Bennu's aqueous alteration, this study presents a high-resolution cathodoluminescence survey of calcites present in clasts and matrix of Cold Bokkeveld CM2 chondrite.

High sensitivity of the CL coupled with the high-spatial resolution of an FEG-SEM is capable to resolve very faint compositional features in calcites that would otherwise have remained invisible at the submicrometer scale using standard BSE imaging. Based on petrographic features, calcites in CM chondrites have been classified into T1 and T2 grains in the literature, both of which being well discriminated by HR-CL panchromatic and hyperspectral analyses. Two types of CL centers have been distinguished: a blue emission band (≈375–425 nm) linked to intrinsic structural defects, possibly induced by lattice distortions, anion vacancies or electron–hole recombination with $CO^3\_$ as holes and Ca^+ as electron, and an orange extrinsic emission at lower energy (≈620 ± 10 nm) in response to Ca-Mn ion substitution. T1 calcites are characterized by a variable intensity of the orange wavelength domain. T1 grains show (oscillatory or patchy) zoning with calcite cores dominated by blue emissions and edges by orange ones. This contrast with the more homogeneous and less intense CL emissions of T2 calcites, characterized by a higher contribution of the blue domain and less pronounced variation around the orange one.

We have also shown that CL characteristics (variability of Mn contents and lattice defects) correlate with different textural environments and oxygen isotope compositions. The T1 calcites characterized by variable CL and peripheral Mn enrichments are always mantled by a rim composed of Fe-S-rich serpentine–tochilinite assemblage, while T2 calcites characterized by homogeneous CL and higher lattice defect are serpentine-free polycrystalline aggregates of calcite grains, containing Fe-Ni sulfide inclusions, and in direct contact with the matrix; such a dichotomy being suggestive of differences in their mode/environment of formation. We posit that changes in Mn content of calcite (orange CL emission intensity) could be better explained by changes in redox-potential (Eh) and pH in the fluid phase rather than by temperature variations. This hydrothermal evolution draws a parallel between the terrestrial serpentinization followed by carbonation processes and the aqueous alteration of CM chondrites, a similarity that certainly deserves to be explored in more detail.

Acknowledgments—C. Monnin, C. Rollion-Bard, A. Verney-Carron, and N. Vigier are thanked for their advice and discussions at different levels of progress of this study. We are grateful for the Loan of NHMW-O1128 Cold Bokkeveld CM2 sample provided by the Natural History Museum Vienna. We also thank V. Batanova (ISTerre, Université Grenoble Alpes) for assistance for EPMPA. We are grateful to two anonymous reviewers for constructive reviews which significantly improved the manuscript, and M. Zolensky for editorial handling. This project was financially supported by ANR O-Return ANR-21-CE49-0005 (G.L. and M.P.). CRHEA and Lagrange laboratories are also acknowledged for their support. This work is, in part, in support of NASA contract NNM10AA11C, the OSIRIS-REx asteroid sample return mission (D. S. Lauretta, principal investigator), as a co-investigator (G.L.) through CNES.

Conflict of Interest Statement—The authors declare that they have no competing interests.

Data Availability Statement—All data needed to evaluate the conclusions in the paper are present in the paper and in the supplementary material. Additional data related to this paper may be requested from the authors.

Editorial Handling—Dr. Michael Zolensky

REFERENCES

Alexander, C. M. O'D., Bowden, R., Fogel, M. L., and Howard, K. T. 2015. Carbonate Abundances and Isotopic Compositions in Chondrites. *Meteoritics & Planetary Science* 50: 810–833.

Bach, W., Paulick, H., Garrido, C. J., Ildefonse, B., Meurer, W. P., and Humphris, S. E. 2006. Unraveling the Sequence of Serpentinization Reactions: Petrography, Mineral Chemistry, and Petrophysics of Serpentinites from MAR 15° N (ODP Leg 209, Site 1274). *Geophysical Research Letters* 33: L13306.

Barker, S. L. L., and Cox, S. F. 2011. Oscillatory Zoning and Trace Element Incorporation in Hydrothermal Minerals: Insights from Calcite Growth Experiments. *Geofluids* 11: 48–56.

Barnaby, R. J., and Rimstidt, J. D. 2014. Redox Conditions of Calcite Cementation Interpreted from Mn and Fe Contents of Authigenic Calcites. *Geological Society of America Bulletin* 101: 795–804.

Barnes, J. D., Paulick, H., Sharp, Z. D., Bach, W., and Beaudoin, G. 2009. Stable Isotope (δ^{18}O, δ D, δ^{37}Cl) Evidence for Multiple Fluid Histories in Mid-Atlantic Abyssal Peridotites (ODP Leg 209). *Lithos* 110: 83–94.

Binzel, R. P., DeMeo, F. E., Burt, B. J., Cloutis, E. A., Rozitis, B., Burbine, T. H., Campins, H., et al. 2015. Spectral Slope Variations for OSIRIS-REx Target

19455100, 0, Downloaded from https://onlinelibrary.wiley.com/doi/10.1111/maps.14225 by Universite Cote D'azur, Wiley Online Library on [11/06/2024]. See the Terms and Conditions (https://onlinelibrary.wiley.com/terms-and-conditions) on Wiley Online Library for rules of use; OA articles are governed by the applicable Creative Commons License

Asteroid (101955) Bennu: Possible Evidence for a Fine-Grained Regolith Equatorial Ridge. *Icarus* 256: 22–29.

Bischoff, A., Ebert, S., Metzler, K., and Lentfort, S. 2017. Breccia Classification of CM Chondrites (Abstract #6089). *Meteoritics & Planetary Science* 52: A26.

Brearley, A. J. 2006. The Action of Water. In *Meteorites and the Early Solar System II*, edited by D. S. Lauretta, and H. Y. McSween, Jr., 587–624. Tucson, AZ: The University of Arizona Press.

Brearley, A. J., and Hutcheon, I. D. 2002. Carbonates in the Y-791198 CM2 Chondrite: Zoning and Mn-Cr Systematic. *Meteoritics & Planetary Science* 37: A23.

Budd, D. A., Hammes, U., and Ward, B. 2000. Cathodoluminescence in Calcite Cements: New Insights on Pb and Zn Sensitizing, Mn Activation, and Fe Quenching at Low Trace Element Concentrations. *Journal of Sedimentary Research* 70: 217–226.

Calderón, T., Aguilar, M., Jaque, F., and Coy-Yll, R. 1984. Thermoluminescence from Natural Calcites. *Journal of Physics C: Solid State Physics* 17: 2027–38.

Chapoulie, R., Cazenave, S., and Cerepi, A. 2005. Contribution of High-Resolution Cathodoluminescence to the Meteoric Diagenesis in Sedimentary Carbonates. *Comptes Rendus Geoscience* 337: 337–346.

Clayton, R. N., and Mayeda, T. K. 1984. The Oxygen Isotope Record in Murchison and Other Carbonaceous Chondrites. *Earth and Planetary Science Letters* 67: 151–161.

Clog, M., Lindgren, P., Modestou, S., McDonald, A., Tait, A., Donnelly, T., Mark, D., and Lee, M. 2024. Clumped Isotope and $\Delta^{17}O$ Measurements of Carbonates in CM Carbonaceous Chondrites: New Insights into Parent Body Thermal and Fluid Evolution. *Geochimica et Cosmochimica Acta* 369: 1–16.

De Leuw, S., Rubin, A. E., and Wasson, J. T. 2010. Carbonates in CM Chondrites: Complex Formational Histories and Comparison to Carbonates in CI Chondrites: Carbonates in CM Chondrites. *Meteoritics & Planetary Science* 45: 513–530.

DellaGiustina, D. N., Burke, K. N., Walsh, K. J., Smith, P. H., Golish, D. R., Bierhaus, E. B., Ballouz, R.-L., and Becker, T. L. 2021. Variations in Color and Reflectance on the Surface of Asteroid (101955) Bennu. *Science* 370.

Doyle, P., Jogo, K., Nagashima, K., Krot, A. N., Wakita, S., Ciesla, F. J., and Hutcheon, I. D. 2015. Early Aqueous Activity on the Ordinary and Carbonaceous Chondrite Parent Bodies Recorded by Fayalite. *Nature Communications* 6: 7444.

Dromgoole, E. L., and Walter, L. M. 1990. Iron and Manganese Incorporation into Calcite: Effects of Growth Kinetics, Temperature and Solution Chemistry. *Chemical Geology* 81: 311–336.

Farsang, S., Franchi, I. A., Zhao, X., Raub, T. D., Redfern, S. A. T., and Grady, M. M. 2021. Carbonate Assemblages in Cold Bokkeveld CM Chondrite Reveal Complex Parent Body Evolution. *Meteoritics & Planetary Science* 56: 723–741.

Force, E. R., and Maynard, J. B. 1991. Manganese: Syngenetic Deposits on the Margins of Anoxic Basins. In *Sedimentary and Diagenetic Mineral Deposits: A Basin Analysis Approach to Exploration*, 147–159. Littleton, Colorado: Society of Economic Geologists.

Frue-Green, G. L., Connolly, J. A. D., Plas, A., Kelley, D. S., and Grobety, B. 2004. Serpentinization of the Oceanic Peridotites: Implication for Geochemical Cycles and Biological Activity. *Geophysical Monograph Series* 144: 119–136.

Fuchs, L. H., Olsen, E., and Jensen, K. J. 1973. Mineralogy, Mineral-Chemistry, and Composition of the Murchison (C2) Meteorite. *Smithsonian Contributions to the Earth Sciences* 10: 1–39.

Fujiya, W., Aoki, Y., Ushikubo, T., Hashizume, K., and Yamaguchi, A. 2020. Carbon Isotopic Evolution of Aqueous Fluids in CM Chondrites: Clues from In-Situ Isotope Analyses within Calcite Grains in Yamato-791198. *Geochimica et Cosmochimica Acta* 274: 246–260.

Fujiya, W., Sugiura, N., Hotta, H., Ichimura, K., and Sano, Y. 2012. Evidence for the Late Formation of Hydrous Asteroids from Young Meteoritic Carbonates. *Nature Communications* 3: 627.

Fujiya, W., Sugiura, N., Marrocchi, Y., Takahata, N., Hoppe, P., Shirai, K., Sano, Y., and Hiyagon, H. 2015. Comprehensive Study of Carbon and Oxygen Isotopic Compositions, Trace Element Abundances, and Cathodoluminescence Intensities of Calcite in the Murchison CM Chondrite. *Geochimica et Cosmochimica Acta* 161: 101–117.

Garcia-Guinea, J., Tormo, L., Azumendi, O., Ruiz, J., and Correcher, V. 2011. Strong Calcite-Like Spectra Cathodoluminescence Emission from Allende Meteorite CAI Phases. *Spectroscopy Letters* 44: 516–520.

Garenne, A., Beck, P., Montes-Hernandez, G., Chiriac, R., Toche, F., Quirico, E., Bonal, L., and Schmitt, B. 2014. The Abundance and Stability of "Water" in Type 1 and 2 Carbonaceous Chondrites (CI, CM and CR). *Geochimica et Cosmochimica Acta* 137: 93–112.

Götze, J. 2012. Application of Cathodoluminescence Microscopy and Spectroscopy in Geosciences. *Microscopy and Microanalysis* 18: 1270–84.

Greenwood, R. C., Findlay, R., Martins, R., Steele, R. C. J., Shaw, K. M. M., Morton, E., Savage, P. S., et al. 2023. The Formation and Aqueous Alteration of CM2 Chondrites and their Relationship to CO3 Chondrites: A Fresh Isotopic (O, Cd, Cr, Si, Te, Ti, and Zn) Perspective from the Winchcombe CM2 Fall. *Meteoritics & Planetary Science* 43: 1–24.

Guo, W., and Eiler, J. M. 2007. Temperatures of Aqueous Alteration and Evidence for Methane Generation on the Parent Bodies of the CM Chondrites. *Geochimica et Cosmochimica Acta* 71: 5565–75.

Habermann, D., Neuser, R. D., and Richter, D. K. 1998. Low Limit of Mn^{2+}-Activated Cathodoluminescence of Calcite: State of the Art. *Sedimentary Geology* 116: 13–24.

Hamilton, V. E., Simon, A. A., Christensen, P. R., Reuter, D. C., Clark, B. E., Barucci, M. A., Bowles, N. E., et al. 2019. Evidence for Widespread Hydrated Minerals on Asteroid (101955) Bennu. *Nature Astronomy* 3: 332–340.

Howard, K. T., Alexander, C. M. O'D., Schrader, D. L., and Dyl, K. A. 2015. Classification of Hydrous Meteorites (CR, CM and C2 Ungrouped) by Phyllosilicate Fraction: PSD-XRD Modal Mineralogy and Planetesimal Environments. *Geochimica et Cosmochimica Acta* 149: 206–222.

Howard, K. T., Benedix, G. K., Bland, P. A., and Cressey, G. 2009. Modal Mineralogy of CM2 Chondrites by X-Ray Diffraction (PSD-XRD). Part 1: Total Phyllosilicate Abundance and the Degree of Aqueous Alteration. *Geochimica et Cosmochimica Acta* 73: 4576–89.

Howard, K. T., Benedix, G. K., Bland, P. A., and Cressey, G. 2011. Modal Mineralogy of CM Chondrites by X-Ray Diffraction (PSD-XRD): Part 2. Degree, Nature and Settings of Aqueous Alteration. *Geochimica et Cosmochimica Acta* 75: 2735–51.

19455100, 0, Downloaded from https://onlinelibrary.wiley.com/doi/10.1111/maps.14225 by Universite Cote D'azur, Wiley Online Library on [11/06/2024]. See the Terms and Conditions (https://onlinelibrary.wiley.com/terms-and-conditions) on Wiley Online Library for rules of use; OA articles are governed by the applicable Creative Commons License

Kaplan, H. H., Lauretta, D. S., Simon, A. A., Hamilton, V. E., DellaGiustina, D. N., Golish, D. R., Reuter, D. C., et al. 2020. Bright Carbonate Veins on Asteroid (101955) Bennu: Implications for Aqueous Alteration History. *Science* 370: 6517.

Kimura, M., Imae, N., Komatsu, M., Barrat, J.-M., Greenwood, R. C., Yamaguchi, A., and Noguchi, T. 2020. The most Primitive CM Chondrites, Asuka 12085, 12169, and 12236, of Subtypes 3.0–2.8: Their Characteristic Features and Classification. *Polar Science* 26: 100565.

King, A. J., Schofield, P. F., and Russell, S. S. 2021. Thermal Alteration of CM Carbonaceous Chondrites: Mineralogical Changes and Metamorphic Temperatures. *Geochimica et Cosmochimica Acta* 298: 167–190.

Lauretta, D. S. 2023. "From Asteroid to Earth: First Results from the OSIRIS-REx Mission and Implications for Planetary Science." In AGU Meeting 2023, abstract P14A-01.

Lauretta, D. S., Adam, C. D., Allen, A. J., Ballouz, R. L., Barnouin, O. S., Becker, K. J., Becker, T., et al. 2022. Spacecraft Sample Collection and Subsurface Excavation of Asteroid (101955) Bennu. *Science* 377: 285–291.

Lee, M. R., and Ellen, R. 2008. Aragonite in the Murray (CM2) Carbonaceous Chondrite: Implications for Parent Body Compaction and Aqueous Alteration. *Meteoritics & Planetary Science* 43: 1219–31.

Lee, M. R., Lindgren, P., and Sofe, M. R. 2014. Aragonite, Breunnerite, Calcite and Dolomite in the CM Carbonaceous Chondrites: High Fidelity Recorders of Progressive Parent Body Aqueous Alteration. *Geochimica et Cosmochimica Acta* 144: 126–156.

Lee, M. R., Lindgren, P., Sofe, M. R., Alexander, C. M. O'D., and Wang, J. 2012. Extended Chronologies of Aqueous Alteration in the CM2 Carbonaceous Chondrites: Evidence from Carbonates in Queen Alexandra Range 93005. *Geochimica et Cosmochimica Acta* 92: 148–169.

Lee, M. R., Martin, R. W., Trager-Cowan, C., and Edwards, P. R. 2005. Imaging of Cathodoluminescence Zoning in Calcite by Scanning Electron Microscopy and Hyperspectral Mapping. *Journal of Sedimentary Research* 75: 313–322.

Lee, M. R., Sofe, M. R., Lindgren, P., Starkey, N. A., and Franchi, I. A. 2013. The Oxygen Isotope Evolution of Parent Body Aqueous Solutions as Recorded by Multiple Carbonate Generations in the Lonewolf Nunataks 94101 CM2 Carbonaceous Chondrite. *Geochimica et Cosmochimica Acta* 121: 452–466.

Lentfort, S., Bischoff, A., Ebert, S., and Patzek, M. 2020. Classification of CM Chondrite Breccias—Implications for the Evaluation of Samples from the OSIRIS-REx and Hayabusa 2 Missions. *Meteoritics & Planetary Science* 56: 127–147.

Leroux, H., Cuvillier, P., Zanda, B., and Hewins, R. H. 2015. GEMS Like Material in the Matrix of the Paris Meteorite and the Early Stages of Alteration of CM Chondrites. *Geochimica et Cosmochimica Acta* 170: 247–265.

Libourel, G., Ganino, C., Delbo, M., Niezgoda, M., Remy, B., Aranda, L., and Michel, P. 2021. Network of Thermal Cracks in Meteorites Due to Temperature Variations: New Experimental Evidence and Implications for Asteroid Surfaces. *Monthly Notices of the Royal Astronomical Society* 500: 1905–20.

Libourel, G., Nagashima, K., Portail, M., and Krot, A. N. 2022. Oxygen Isotope Variations in Mg-Rich Olivines from Type I Chondrules in Carbonaceous Chondrites. *Geochimica et Cosmochimica Acta* 319: 73–93.

Libourel, G., and Portail, M. 2018. Chondrules as Direct Thermochemical Sensors of Solar Protoplanetary Disk Gas. *Science Advances* 4(7): eaar3321.

Lindgren, P., Lee, M. R., Sofe, M. R., and Zolensky, M. E. 2013. Clasts in the CM2 Carbonaceous Chondrite Lonewolf Nunataks 94101: Evidence for Aqueous Alteration Prior to Complex Mixing. *Meteoritics & Planetary Science* 48: 1074–90.

Lindgren, P., Lee, M. R., Sparkes, R., Greenwood, R. C., Hanna, R. D., Franchi, I. A., King, A. J., et al. 2020. Signatures of the Post-Hydration Heating of Highly Aqueously Altered CM Carbonaceous Chondrites and Implications for Interpreting Asteroid Sample Returns. *Geochimica et Cosmochimica Acta* 289: 69–92.

Lindgren, P., Lee, M. R., Starkey, N. A., and Franchi, I. A. 2017. Fluid Evolution in CM Carbonaceous Chondrites Tracked through the Oxygen Isotopic Compositions of Carbonates. *Geochimica et Cosmochimica Acta* 204: 240–251.

Machel, H. G. 2000. Application of Cathodoluminescence to Carbonate Diagenesis. In *Cathodoluminescence in Geosciences*, edited by M. Pagel, V. Barbin, P. Blanc, and D. Ohnenstetter, 271–301. Berlin: Springer.

Maynard, J. B. 2003. Manganiferous Sediments, Rocks, and Ores. In *Treatise on Geochemistry 7*, edited by H. D. Holland, and K. K. Turekian, 298–307. Oxford: Elsevier-Pergamon.

McSween, H. Y., Emery, J. P., Rivkin, A. S., Toplis, M. J., Castillo-Rogez, J. C., Prettyman, T. H., Cristina De Sanctis, M., Pieters, C. M., Raymond, C. A., and Russell, C. T. 2018. Carbonaceous Chondrites as Analogs for the Composition and Alteration of Ceres. *Meteoritics & Planetary Science* 53: 1793–1804.

Metzler, K., Bischoff, A., and Stöffler, D. 1992. Accretionary Dust Mantles in CM Chondrites: Evidence for Solar Nebula Processes. *Geochimica et Cosmochimica Acta* 56: 2873–97.

Mevel, C. 2003. Serpentinization of Abyssal Peridotites at Mid-Ocean Ridges. *Comptes Rendus Geoscience* 335: 825–852.

Miyamoto, M. 1991. Thermal Metamorphism of CI and CM Carbonaceous Chondrites: An Internal Heating Model. *Meteoritics & Planetary Science* 26: 111–15.

Nakamura, T., and Nakamuta, Y. 1996. X-Ray Study of PCP from the Murchison CM Carbonaceous Chondrites. *Proceedings of the National Institute of Polar Research Symposium on Antarctic Meteorites* 9: 37–50.

Nozaki, W., Nakamura, T., and Noguchi, T. 2006. Bulk Mineralogical Changes of Hydrous Micrometeorites during Heating in the Upper Atmosphere at Temperatures below 1000°C. *Meteoritics & Planetary Science* 41: 1095–1114.

Pagel, M., Barbin, V., Blanc, P., and Ohnenstetter, D. 2000. *Cathodoluminescence in Geosciences*. Berlin: Springer.

Palmer, E. E., and Lauretta, D. S. 2011. Aqueous Alteration of Kamacite in CM Chondrites. *Meteoritics & Planetary Science* 46: 1587–1607.

Picazo, S., Malvoisin, B., Baumgartner, L., and Bouvier, A. S. 2020. Low Temperature Serpentinite Replacement by Carbonates during Seawater Influx in the Newfoundland Margin. *Minerals* 10: 184.

Pignatelli, I., Marrocchi, Y., Mugnaioli, E., Bourdelle, F., and Gounelle, M. 2017. Mineralogical, Crystallographic and Redox Features of the Earliest Stages of Fluid Alteration in CM Chondrites. *Geochimica et Cosmochimica Acta* 209: 106–122.

Riciputi, L. R., McSween, H. Y., Jr., Johnson, C. A., and Prinz, M. 1994. Minor and Trace Element Concentrations in Carbonates of Carbonaceous Chondrites, and

19455100, 0, Downloaded from https://onlinelibrary.wiley.com/doi/10.1111/maps.14225 by Universite Cote D'azur, Wiley Online Library on [11/06/2024]. See the Terms and Conditions (https://onlinelibrary.wiley.com/terms-and-conditions) on Wiley Online Library for rules of use; OA articles are governed by the applicable Creative Commons License

Implications for the Compositions of Coexisting Fluids. *Geochimica et Cosmochimica Acta* 58: 1343–51.
Rosenberg, N. D., Browning, L., and Bourcier, W. L. 2001. Modeling Aqueous Alteration of CM Carbonaceous Chondrites. *Meteoritics & Planetary Science* 36: 239–244.
Roumejon, S., Williams, M. J., and Früh-Green, G. L. 2018. In-Situ Oxygen Isotope Analyses in Serpentine Minerals: Constraints on Serpentinization during Tectonic Exhumation at Slow- and Ultraslow-Spreading Ridges. *Lithos* 323: 156–173.
Rubin, A. E., Trigo-Rodrıguez, J. M., Huber, H., and Wasson, J. T. 2007. Progressive Aqueous Alteration of CM Carbonaceous Chondrites. *Geochimica et Cosmochimica Acta* 71: 2361–82.
Russell, M. J., Hall, A. J., Boyce, A. J., and Fallick, A. E. 2005. On Hydrothermal Convection Systems and the Emergence of Life. *Economic Geology* 100: 419–438.
Scicchitano, M. R., Lafay, R., Valley, J. W., Kita, N. T., and Nachlas, W. O. 2022. Protracted Hydrothermal Alteration Recorded at the Microscale in the Chenaillet Ophicarbonates (Western Alps): Insights from in situ $\delta^{18}O$ Thermometry in Serpentine, Carbonate and Magnetite. *Geochimica et Cosmochimica Acta* 318: 144–164.
Seyfried, W. E., Jr., Foustoukos, D. I., and Fu, Q. 2007. Redox Evolution and Mass Transfer during Serpentinization: An Experimental and Theoretical Study at 200°C, 500 bar with Implications for Ultramafic-Hosted Hydrothermal Systems at Mid-Ocean Ridges. *Geochimica et Cosmochimica Acta* 71: 3872–86.
Sofe, M. R. 2013. "The Oldest Carbonate Minerals on Earth: Insights into the Early History of the Solar System." PhD thesis, University of Glasgow. https://theses.gla.ac.uk/4107/.
Suttle, M. D., Daly, L., Jones, R. H., Jenkins, L., Van Ginneken, M., Mitchell, J. T., Bridges, J. C., et al. 2023. The Winchcombe Meteorite—A Regolith Breccia from a Rubble Pile CM Chondrite Asteroid. *Meteoritics & Planetary Science* 58: 1–25.
Suttle, M. D., King, A. J., Schofield, P. F., Bates, H., and Russel, S. S. 2021. The Aqueous Alteration of CM Chondrites, a Review. *Geochimica et Cosmochimica Acta* 299: 219–225.
Telus, M., Hauri, E. H., and Wang, J. 2019. Calcite and Dolomite Formation in the CM Parent Body: Insight from In Situ C and O Isotope Analyses. *Geochimica et Cosmochimica Acta* 260: 275–291.
Toffolo, M. B., Ricci, G., Caneve, L., and Kaplan-Ashiri, I. 2019. Luminescence Reveals Variations in Local Structural Order of Calcium Carbonate Polymorphs Formed by Different Mechanisms. *Scientific Reports* 9: 16170.
Tomeoka, K., and Buseck, P. R. 1985. Indicators of Aqueous Alteration in CM Carbonaceous Chondrites: Microtextures of a Layered Mineral Containing Fe, S, O and Ni. *Geochimica et Cosmochimica Acta* 49: 2149–63.
Tyra, M., Brearley, A., and Guan, Y. 2016. Episodic Carbonate Precipitation in the CM Chondrite ALH 84049: An Ion Microprobe Analysis of O and C Isotopes. *Geochimica et Cosmochimica Acta* 175: 195–207.
Tyra, M. A., Farquhar, J., Guan, Y., and Leshin, L. A. 2012. An Oxygen Isotope Dichotomy in CM2 Chondritic Carbonates—A SIMS Approach. *Geochimica et Cosmochimica Acta* 77: 383–395.
Tyra, M. A., Farquhar, J., Wing, B. A., Benedix, G. K., Jull, A. J. T., Jackson, T., and Thiemens, M. H. 2007. Terrestrial Alteration of Carbonate in a Suite of Antarctic CM Chondrites: Evidence from Oxygen and Carbon Isotopes. *Geochimica et Cosmochimica Acta* 71: 782–795.
Vacher, L. G., Marrocchi, Y., Villeneuve, J., Verdier-Paoletti, M. J., and Gounelle, M. 2017. Petrographic and C & O isotopic characteristics of the earliest stages of aqueous alteration of CM chondrites. *Geochimica et Cosmochimica Acta* 213: 271–290.
Vacher, L. G., Piralla, M., Gounelle, M., Bizzarro, M., and Marrocchi, Y. 2019. Thermal Evolution of Hydrated Asteroids Inferred from Oxygen Isotopes. *The Astrophysical Journal Letters* 882: L20.
Vacher, L. G., Truche, L., Faure, F., Tissandier, L., Mosser-Ruck, R., and Marrocchi, Y. 2019. Deciphering the Conditions of Tochilinite and Cronstedtite Formation in CM Chondrites from Low Temperature Hydrothermal Experiments. *Meteoritics & Planetary Science* 54: 1870–89.
Velbel, M. A., and Palmer, E. E. 2011. Fine-Grained Serpentine in CM2 Carbonaceous Chondrites and its Implications for the Extent of Aqueous Alteration on the Parent Body: A Review. *Clays and Clay Minerals* 59: 416–432.
Velbel, M. A., Tonui, E. K., and Zolensky, M. E. 2012. Replacement of Olivine by Serpentine in the Carbonaceous Chondrite Nogoya (CM2). *Geochimica et Cosmochimica Acta* 87: 117–135.
Velbel, M. A., Tonui, E. K., and Zolensky, M. E. 2015. Replacement of Olivine by Serpentine in the Queen Alexandra Range 93005 Carbonaceous Chondrite (CM2): Reactant–Product Compositional Relations, and Isovolumetric Constraints on Reaction Stoichiometry and Elemental Mobility during Aqueous Alteration. *Geochimica et Cosmochimica Acta* 148: 402–425.
Verdier-Paoletti, M. J., Marrocchi, Y., Avice, G., Roskosz, M., Gurenko, A., and Gounelle, M. 2017. Oxygen Isotope Constraints on the Alteration Temperatures of CM Chondrites. *Earth and Planetary Science Letters* 458: 273–281.
Visser, R., John, T., Whitehouse, M. J., Patzek, M., and Bischoff, A. 2020. A Short-Lived ^{26}Al Induced Hydrothermal Alteration Event in the Outer Solar System: Constraints from Mn/Cr Ages of Carbonates. *Earth and Planetary Science Letters* 547: 116440.
Zolensky, M. E., Mittlefehldt, D. W., Lipschutz, M. E., Wang, M.-S., Clayton, R. N., Mayeda, T. K., Grady, M. M., Pillinger, C., and Barber, D. 1997. CM Chondrites Exhibit the Complete Petrologic Range from Type 2 to 1. *Geochimica et Cosmochimica Acta* 61: 5099–5115.

SUPPORTING INFORMATION

Additional supporting information may be found in the online version of this article.

FIGURE S1. Secondary electrons' SEM image of C4 calcite showing beam damages induced by EMPA X-ray map after 14 h of analyses, corresponding to Mn X-ray map presented in Figure 6.

FIGURE S2. Blended X-ray elemental map in Ca (red), Fe (green), and Al Kα (blue) and BSE map by SEM of the NHMW-O1128 Cold Bokkeveld CM2 thin section. Cold Bokkeveld is a chondrite breccia hosting various clast of different lithology, size, and degree of alteration.

19455100, 0, Downloaded from https://onlinelibrary.wiley.com/doi/10.1111/maps.14225 by Universite Cote D'azur, Wiley Online Library on [11/06/2024]. See the Terms and Conditions (https://onlinelibrary.wiley.com/terms-and-conditions) on Wiley Online Library for rules of use; OA articles are governed by the applicable Creative Commons License

Some of these clasts have been identified with letters A–H and their borders highlighted with blue lines. The various degrees of alteration recorded by each of these clasts can be simply apprehended by the intensity of iron variations of the X-ray map (green color), here used as an indicator of "FeO"/SiO_2 ratio of TCIs following the method proposed by Rubin et al. (2007). Calcite grains (orange-pink) are present both in clast and matrix. Red dotted square represents the location of Figure 2.

FIGURE S3. Image processing procedure to produce a map showing the variability of the Fe/Si ratio from Fe X-ray and Si-X-ray SEM maps (a) using ImageJ@ software.

FIGURE S4. Chemical composition of representative T1 and T2 calcites analyzed by EMPA and their variations.

FIGURE S5. Deconvolution and peak fitting of SEM-CL spectra of representative T1 and T2 calcites from Cold Bokkeveld.

FIGURE S6. Backscattered electron and panchromatic CL images of more than 80 calcite grains belonging to different clasts or in the matrix of Cold Bokkeveld CM2 chondrite (see Figure 1 for location and numbering of the various clasts).

TABLE S1. The chemical composition of representative T1 and T2 calcites from Cold Bokkeveld and corresponding area of cathodoluminescence (CL) spectra measured 620 nm and 400 nm wavelength, respectively (see text). Analyses in bold are those obeying the stoichiometry of calcite, including their minor elements, e.g., (Ca, Mg, Fe, Mn)CO_3 ($54 < CaO < 58$ wt %), and those used for quantification in this study.

19455100, 0, Downloaded from https://onlinelibrary.wiley.com/doi/10.1111/maps.14225 by Universite Cote D'azur, Wiley Online Library on [11/06/2024]. See the Terms and Conditions (https://onlinelibrary.wiley.com/terms-and-conditions) on Wiley Online Library for rules of use; OA articles are governed by the applicable Creative Commons License